Structural Application of ash in concrete

Department of Civil Engineering

Technical University of Denmark

DTU Civil Engineering
Department of Civil Engineering

Abstract

Introduction

Worldwide the production of cement causes 5% of the total CO_2 emissions [1]. In Denmark 2 million tons of cement is used every year [2] yielding 1.8 million tons CO_2 emissions [3]. This is a substantial amount for one single production, why it is desirable to lower the demand for cement. Cement is mostly used for concrete and is the adhesive component in concrete, why it also is responsible for main strength in the concrete. Some additives such as fly ash and microsilica do also provide strength for concrete. From this, the idea rose to use sewage sludge ash (SSA), not only as an additive, but to replace a substantial amount of cement with SSA. SSA is a waste product, which for the time being is being deposited; as no better solution is known.

If it is possible to use SSA to replace cement in concrete, it is, thus possible to reduce two environmental problems with one solution.

Preceding projects has been made at DTU Civil Engineering, with investigations on mortar (concrete without a large fraction of stone) concerning: strength, chemical analysis, durability, workability etc. However this project is the first to test the SSA in concrete. The aim is to see the effects on the load carrying capacity for two types of structural members used in the construction industry: Beams and columns.

Methods

A reference concrete is designed, and from this two types of SSA-concretes are made, with respectively 25 and 50 mass-% cement replaced with SSA. A trial casting is made to make sure it is possible to cast the concrete in a satisfactory way. In the data processing the two SSA concretes are compared to the reference concrete.

The two experiments performed are a beam test, where the loading is perpendicular to the longitudinal direction of the beam, and a column test with loading parallel to the longitudinal direction. To get the strength properties of the concrete and reinforcement-steel compression tests for the concrete and tensile tests for the steel are performed.

Results

The compression test for the concrete shows a loss in strength when increasing the amount of SSA. This is expected and is also what previous projects have shown.

The column test shows a decrease of 6% in carrying capacity when replacing 25 % of the cement with SSA, and a decrease of 25 % when replacing 50% of the cement with SSA. In the beam test, the moment capacity does not decrease significantly when replacing cement with SSA. Even at 50% replacement the moment capacity decrease is less than 5%.

Conclusion

From this project it can be concluded that adding SSA to concrete is a possibility with regards to the bearing capacity of beams and columns. The capacities of the members are sufficient to be used in real projects, especially for the beams, which have an insignificant reduction in carrying capacity though lowering the compression strength of the concrete.

The durability demand of the characteristic compressive strength for concrete in passive exposure classes is only 12MPa [4]. The concrete with 50% cement replaced with SSA also fulfils this demand. About 2/3^{rds} [5] of all concrete in Denmark is used in passive exposure class. This gives a potential saving of CO_2 of up to 1/3rd of all cement related CO_2 emissions corresponding to a total reduction in CO_2 emissions of 1.66 %.

Preface

The purpose of this report is to evaluate four students taking a special course at the Department of Civil Engineering at the Technical University of Denmark. The report is made by Martin Riis Iskau, Bjarne Due Olsen, Jeppe Søbye Andreasen and Jonatan Stær Nissen. The special course is stipulated to 10 ECTS points and is conducted in the spring semester of 2015.

The report concerns casting, testing and evaluation of concrete beams and columns containing sewage sludge ash (SSA), compared to reference beams and columns cast with a standard concrete.

Special thanks must be given to:

Per Goltermann for being the project advisor and giving helpful guidance throughout the project.

Per Leth regarding concrete casting and reinforcement works.

Robert Svan & Henrik Børglum regarding mechanical aspects of the test setup.

Christian Peter Rasmussen regarding the electronically test setup and measuring technique.

Keld Plougmann & Jørgen Bjørnbak-Hansen regarding special fittings of the couplings for the column experiment

With regards to responsibility of this project and report, the group is equally responsible for each chapter in this report.

(Front page photo: Cylinder specimens after demoulding)

Martin Riis Iskau, s103553

Bjarne Due Olsen, s103616

Jeppe Søbye Andreasen, 103603

Jonathan Stær Nissen,s103589

Project Composition

This report is composed of 7 sections and 9 appendixes. Apart from the appendixes in the appendix report, a collection of electronic appendixes are to be found in the zip file. These electronic appendixes includes video documentation, calculation sheets and scripts.

Sources in the bibliography is presented by; writer, title, publisher and publish year. The sources in the bibliography are listed in the order they are referred to.

Figures are listed by section number followed by sequential number.

Tables are listed by section number followed by sequential number.

Equations are listed by section number followed by sequential numbers.

For dimensioning calculations and post-processing the programs Microsoft Excel, Maple and Matlab are used. For figures the programs Autocad and Microsoft paint is used. The report is written with Microsoft word and LaTex.

The program Benchlink Data Logger is used In the four point bending experiments for the beams and the compression tests of the concrete cylinders. The program Wawemaker Editor is used in the tensile tests of the reinforcement. Both Benchlink Data Logger and Wawemaker Editor are used in the column experiments.

Symbols and their meaning are listed in the symbol-legend in the beginning of the report.

Table of contents

Table of figures

Table of tables

Symbol-legend

a	Distance between loading points
A	Cross section area
A_c	Concrete cross section area
A_{cp}	Plastic compression zone area
A_{piston}	Piston cross section area
A_s	Tension reinforcement cross section area
A_{sc}	Compression reinforcement cross section area
c	Cover layer
c/c	Center to center
d	Effective height of cross section
d_{sc}	Distance from upper edge to center of compression reinforcement
E	Young's modulus / Modulus of elasticity
E_a	Activation energy
E_s	Modulus of elasticity steel
e	Eccentricity
F	Force
F_c	Compression force
F_s	Tension force
f_{ck}	Characteristic strength of concrete
f_{cm}	Mean compressive strength of concrete
f_y	Yield strength of steel
f_{yk}	Characteristic yield strength of steel
h	Cross section height
$H(\theta)$	Relative hardening velocity
$h_{c,eff}$	Effective height of concrete in tension around the reinforcement
K	Cement type constant or Dimensionless size
k	Dimensionless size
L	Length
L_{arch}	Travelled arch length
L_s	Buckling length
M	Maturity/Moment
M_{FC}	Moment at fully cracked cross section
M_C	Moment at partly cracked cross section
M_y	Moment at reinforcement yielding
M_u	Moment at compression failure
n	Number
N	Normal force
p	Pressure
R	Gas constant
r	Curvature radius
Δs	Displacement

$S_{r,max}$	Maximum crack distance
$S_{\emptyset}$	Distance between tensile reinforcement
u	Deflection
ΔU	Voltage
w	Width
w/c	water/cement ratio
$\emptyset$	Reinforcement diameter
x	Compression zone height, displacement or inner moment distance – depending on the formula
y	Plastic compression zone height or function variable

Greek letters

α	Relationship between the steel and concrete Yong's modulus – The curvature parameter – The angle of a tangent (at a segment of a cicle used at the curvature calculation) – The cement type - Constant
ε	Strain
ε_{cu2}	Concrete strain at fracture at pure compression
ε_{cu3}	Concrete strain at fracture considering rectangular stress distribution at bending
ε_s	Tension reinforcement strain
ε_{sc}	Compression reinforcement strain
ε_y	Yield strain
ε_u	Ultimate strain
η	Dimensionless size
θ	Temperature
κ	Curvature
λ	Reduction factor from concrete compression zone to plastic concrete compression zone by rectangular stress distribution, 0.8 for rectangular compression zones
μ	Mean value (statistical)
σ	Stress or standard deviation (statistical)
$\sigma_{p0.2}$	Stress at 0.2% strain
σ_s	Tension reinforcement stress
σ_{sc}	Compression reinforcement stress
τ	Characteristic time constant

1 Introduction

Because of the industrialization of the world the humanity has emitted a great amount of CO_2 to the atmosphere increasing the concentration of greenhouse gasses. Worldwide the production of cement causes 5% of the total CO_2 emissions [6]. In Denmark 2 million tons of cement is used every year [2] yielding 1.8 million tons CO_2 emissions [3]. This is a substantial amount from the production of one specific product. As a result it is desirable to lower the amount of cement produced.

Sewage sludge is a waste product from the wastewater treatment plant. The sludge is burned to ash (SSA) to save space when depositing. At these deposit sites the SSA leads to environmental problems as it takes a long time to decompose and contains e.g. heavy metals. The global population has grown from ca. 3 billion people in 1960 to 7.2 billion in 2013. The growth is expected to continue for the years to come, hence the problem with the deposit of the SSA will only grow bigger as times goes by [7].

By replacing some of the cement in concrete with SSA it is possible to reduce these two environmental problems (CO_2 emissions from cement production and deposit of SSA) with one solution. Furthermore SSA contains amounts of phosphorous which is a scarce resource. It has been shown that the phosphorous can be extracted from the SSA and reused [8].

About 2/3^{rds} [5] of all concrete in Denmark is used in passive exposure class where it can be allowable to replace cement with SSA. This gives a potential saving of CO_2 of up to 1/3rd of all cement related CO_2 emissions corresponding to a total reduction in CO_2 emissions of 1.66 %.

Previous investigation has been carried out concerning cement replaced with SSA. These investigations were made with mortar because of the high dispersion in the results for concrete due to the inhomogeneous mass in concrete. The purpose of this project is to test concrete in a large scale.

In this project specimens are named based on their content of SSA e.g. *25* if 25 % of the cement is replaced with SSA, and their structural purpose. The specimens not containing SSA are referred to as *REF*. Beams are referred to as *B* and columns as *S*. The initial concrete cylinders are referred to as *C0*. The specimens used are shown in Table 1-1.

Table 1-1: Specimen naming

Description	Name	No.
Initial cylinders	C0-REF	1-5
	C0-10	1-5
	C0-20	1-5
	C0-30	1-5
	C0-40	1-5
	C0-50	1-5
Beam cylinders	BC-REF	1-5
	BC-25	1-5
	BC-50	1-5
Column cylinders	SC-REF	1-5
	SC-25	1-5
	SC-50	1-5
Beams	B-REF	1-3
	B-25	1-3
	B-50	1-3
Columns	S-REF	1-3
	S-25	1-3
	S-50	1-3

1.1 Thesis statement

The purpose of this project is to investigate the effect on bearing capacity of reinforced concrete beams and columns when replacing part of the cement with SSA in proportion 1:1 by weight. A secondary aim is to find out if it is possible to replace 50% of the cement with SSA and still obtain a cast-able concrete.

The compressive strength of the concrete must be determined in order to design the beams and columns. It is expected that the compressive strength will decrease when replacing cement with SSA. A tensile test is performed for the reinforcement in order to validate the strength. All investigations of beams and columns are compared to a reference specimen without any SSA added.

The hypothesis is that the compressive strength of the concrete is not decisive in relation to the bearing capacity of the structural elements compared to the steel reinforcement strength. It is expected that the bearing capacity will decrease slightly with a decreasing concrete compressive strength but not significantly.

1.2 Sludge ash origin

The ash used in the project is obtained by burning the dry waste product from treatment of sewage water. The sludge is burned to produce power and reduce the volume of the product for storage. In this project the ash used are produced on the waste water treating facility in Avedøre.

1.2.1 Chemical composition of the sludge ash

The chemical composition of the sludge ash used in the project is shown in Table 1-2 along with a typical chemical composition of fly ash.

Table 1-2: Chemical composition of the SSA vs Fly Ash. The quantities are taken from reports presented in appendix A.1 and A.2.

Main element	Chemical notation	Fly Ash	Sludge ash	SSA without phosphor
Silicon	SiO_2	36-59 %	32 %	40 %
Aluminum	Al_2O_3	20-35 %	9.4 %	11.75 %
Iron	Fe_2O_3	3-19 %	14 %	17.5 %
Calcium	CaO	1-12 %	16 %	20 %
Manganese	MgO	0.7-4.8 %	2.6 %	3.25 %
Titanium	TiO_2	0.5-1.8 %	0.83 %	1.0375 %
Sodium	Na_2O	0.1-3.5 %	0.83 %	1.0375 %
Potassium	K_2O	0.5-6 %	1.6 %	2 %
Phosphor	P_2O_5	-	20 %	-
Sulfur	SO_3	0.1-2%	-	-

When comparing to a typical chemical composition of fly ash it is observed that the SSA contains most of the same components as the fly ash. The main difference is that SSA contains high amounts of phosphorus pentoxide originating from laundry detergents in the wastewater. Phosphor is used in many products in society, mainly fertilizers, and has more value in these products than they will have in concrete. If the extraction of phosphor is possible, it might be useful to extract the phosphorus pentoxide from the ash leaving a product with a chemical composition much closer to that of fly ash. As the chemical composition even without removing the phosphor is still close to that of fly ash, it is therefore expected that SSA may contribute to the final concrete compressive strength.

The SSA contains different amounts of various heavy metals. Many heavy metals are poisonous and are therefore not allowed to end up in constructions. The heavy metals should therefore also be removed from the ash before it is used in concrete.

The SSA is potential a health risk when it is used in the laboratory why a risk assessment has been worked out. This assessment can be seen in appendix A.3

2 Concrete

2.1 Design of the concrete

The concrete is designed in accordance with Bolomey's formula [9].

$$f_{cm} = K \cdot \left(\frac{1}{w/c} - \alpha\right) \tag{2-1}$$

Where:

f_{cm}	is the mean compressive strength
K and α	are constants in relation to the cement type
w/c	is the water/cement-ratio with regards to mass.

The recipe is designed for the reference concrete and the only alteration in the SSA concrete is replacement of a given mass of cement with an equal mass of SSA. This is performed without regarding that the SSA's ability to consume water may be different from the ability of the cement. To obtain a satisfactory slump super plasticizer is added to compensate for this.

No corrections regarding the air content is made since no air entraining agents are used. The cement type used in this project is "*Rapid cement"*. The design mean compressive strength is chosen to be 40 MPa. This is high enough to ensure a sufficient strength when replacing 50% of the cement with SSA.

The water demand is chosen in accordance with the maximum aggregates size [9] and from (2-1). The w/c-ratio can be determined and hence the mass of the cement can be determined. As a final step the sand and stone fractions are determined. The full recipe for $1m^3$ concrete is shown in appendix B.1.

2.2 Maturity

Because this series of experiments are scheduled only to run in the spring semester of 2015 the curing period of the initial concrete samples are shortened to one week instead of the normal curing period of 28 days. This is possible by controlling the temperature in the curing environment. The development is estimated by the term *maturity*, which is dependent on time and temperature. The maturity function is defined in [10] as:

$$M(t) = \int_0^t H\big(\theta(\tau)\big)d\tau \tag{2-2}$$

To ease the calculations, the function can be estimated numerically:

$$M(t) = \sum_0^n H(\theta_i) \cdot \Delta t_i \tag{2-3}$$

Where:

n	the number of steps.
Δt and $d\tau$	is a time period
$H(\theta)$	is the temperature function given as:

$$H(\theta) = \exp\left(\frac{E_a}{R} \cdot \left(\frac{1}{293} - \frac{1}{273 + \theta}\right)\right) \tag{2-4}$$

Where:

θ	is the temperature in Celsius
E_a	is the activation energy, here $\theta > 20°C$ hence $E_a = 33500\frac{J}{mol}$
R	is the gas constant: $8.314\frac{J}{mol \cdot K}$

From (2-3) and (2-4) the maturity M_{20} of concrete at 20°C after 28 days can be calculated. From the maturity the temperature needed for full curing in 7 days can be solved. The obtain temperature needed is $42°C$.

It is not possible to keep the beam and columns in higher temperatures than 20°C. Therefore they have been tested after 21 days.

With (2-3) the expected compressive strength of the reference concrete can be estimated to different dates. It is expected that the strength after 28 days will become 40 MPa for the reference concrete. Thereby the expected compressive strength after 7, 14, 21 and 28 can be estimated, for which the results are shown in Table 2-1. The strength development is also illustrated in Figure 2-1.

$$f_c(M_{20}) = f_{c28} \cdot exp\left(1\left(\frac{1}{\sqrt{M_{20}}} - \frac{1}{\sqrt{28}}\right)\frac{0.7 \cdot f_{c28} + 41}{f_{c28} + 11}\right) \quad (2\text{-}5)$$

Table 2-1: Estimated strength development in 40MPa concrete

Time [Days]	Strength [MPa]	% of f_{c28}
7	31,0	77,4
14	36,0	90,0
21	38,4	96,1
28	40,0	100,0

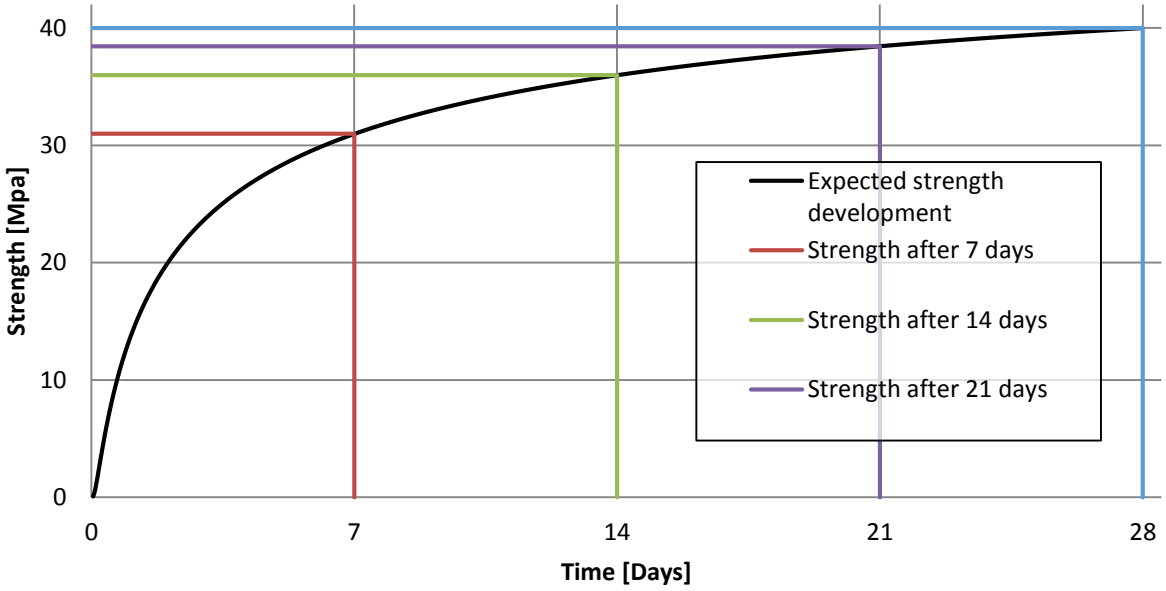

Figure 2-1: Strength development in concrete

It is concluded the testing the beams after 14 or 21 days will yield an acceptable result as long as the compressive strength of the concrete is verified by testing concrete cylinders kept under the same conditions. The experiments have been carried out after 21 days of curing at 20°C.

2.3 Equipment cylinders

- Slump test equipment (cone, rod, and flat steel surface)
- Buckets to measure components into
- Shear force concrete mixer (20 L)
- Shovels.
- Vibrator table
- Five Cylinder molds for each concrete type, with lids and clamps
- Scale for measuring the materials on.
- Compression machine

2.4 Experimental description cylinders

1. The raw materials are measured by weight, into separate containers.
2. The SSA is measured out into a bucket with a closeable lid in no larger amounts than 10 kg at a time. Part of the water is then carefully poured into the SSA to suspend the SSA particles and prevent the SSA from giving off dust.
3. The dry materials are then poured into the concrete mixer and mixed for 300 sec.
4. Plasticizers are added according to appendix B.2.
5. For the reference mix the water is poured in and the concrete is mixed for another 300 sec. for the other concrete mixes the suspended SSA is poured in and the bucket is rinsed with the rest of the mixing water which then is poured into the mixer, and the mixer is run for another 300 sec.
6. A slump test is performed in accordance with [11] for both reference and SSA in order to get an idea of it is possible to cast the concrete to the cylinders. The concrete used for the slump-test is then discarded.
7. The cylinders are filled half way with concrete and vibrated adequately until a smooth surface of the concrete is obtained and no air bubbles are penetrating the surface. The cylinders are then topped off to have sufficient concrete when settling during the final vibration. The cylinders are then vibrated for an adequate amount of time.
8. After the vibration the cylinders are closed. This is performed with the lid, which is moved around in circles until no impurities can be felt between the lid and the cylinder. The lid is then secured on the cylinder with a clamp, cleaned and left for one day of setting in the molds while the longitudinal axes of the cylinders are horizontal to disperse any possible separation in the concrete.
9. After 24 hours the cylinders are de-molded and placed in a container with water. The temperature of the water can be regulated in order to control the hydration process. In this way it is possible to obtain a maturity equivalent to 28 days at 20°C by higher temperature at a shorter time.
10. When the wanted maturity is obtained the cylinders are tested in accordance with [12]. The testing rate in this project is chosen to 0.4 MPa/s.

2.5 Results initial test

For each mixture five cylinders are cast to determine the concrete strength as a mean value. An initial test is performed to investigate the change in strength with a varying SSA content. The results for the initial investigation are summarized in Table 2-2 obtained in appendix C.1 – 6. The missing results from the 10% content mixture are due to faulty use of the test equipment.

Table 2-2: Strength and slump of initial reference concrete test.

Test	1 $[MPa]$	2 $[MPa]$	3 $[MPa]$	4 $[MPa]$	5 $[MPa]$	Mean f_{cm} $[MPa]$	Std. dev. $[MPa]$	Slump [mm]
C0-REF	33.83	44.02	24.85	26.21	39.28	**33.64**	8.25	200
C0-10	32.46	33.10		32.73		**32.76**	0.32	80
C0-20	32.22	32.16	30.34	32.9	31.45	**31.81**	0.97	40
C0-30	25.51	26.00	26.00	24.68	20.93	**24.62**	2.13	40
C0-40	22.69	22.34	22.83	21.84	23.69	**22.68**	0.68	20
C0-50	17.92	16.52	17.46	17.70	18.75	**17.67**	0.81	10

The results from the initial performance test are used for further determination of the most suitable SSA content for beam/column testing. Chosen SSA contents are 25 and 50% which appears in the following tables.

The results of the concrete compressive tests are shown in Table 2-3 for the beam concrete cylinders and in Table 2-4 for the column concrete cylinders.

Table 2-3: Strength and slump of beam concrete test full results in appendix C.7-9.

Test	1 $[MPa]$	2 $[MPa]$	3 $[MPa]$	4 $[MPa]$	5 $[MPa]$	Mean f_{cm} $[MPa]$	Std. dev. $[MPa]$	Slump [mm]
BC-REF	42.51	45.12	40.29	44.63	46.55	**43.82**	2.45	200
BC-25	44.90	41.62	45.49	44.35	40.36	**43.34**	2.23	60
BC-50	23.05	21.09	15.49	22.30	21.83	**20.75**	3.03	50

Table 2-4: Strength and slump of column concrete test full results in appendix C.10-11.

Test	1 $[MPa]$	2 $[MPa]$	3 $[MPa]$	4 $[MPa]$	5 $[MPa]$	Mean f_{cm} $[MPa]$	Std. dev. $[MPa]$	Slump [mm]
SC-REF	41.58	44.25	49.09	36.43	40.94	**42.94**	4.65	45
SC-25	39.72	40.24	39.64	34.71	35.96	**38.05**	2.53	25
SC-50	20.49	25.80	27.67	27.89	24.84	**25.34**	3.00	25

2.6 Result evaluation

2.6.1 Initial test

From the initial compressive test it is evident that the concrete strength is reduced with increased SSA content. The compressive strength is above the acceptable limit for passive exposure class [4] of $f_{ck} = 12\ MPa$. It is noted that the reference mixture has not reached the $40\ MPa$ design strength for all the cylinders. These cylinders were not initially rotated horizontally as prescribed in the casting process, but after a few hours. This means some of the initial strength may have been lost due to disturbances in the initial settled concrete in the cylinders. Another issue is the cylinder molds, which doesn't release easy from the concrete at de-molding after 24 hours.

In the initial test the same amount of super plasticizers (0.3% of cement weight) are added to all the recipes which resulted in a very slump reference sample and some very stiff SSA samples especially with high content of SSA. Therefore the concentrations are differentiated subsequently. It is generally observed that the SSA influences the slump of the concrete significantly and increases the need for vibration and super plasticizers. This must be taken into consideration when choosing to use SSA to replace cement in future concrete designs.

2.6.2 Beam test

As seen from Table 2-3 the compressive strength of BC-REF and BC-25 is not significantly different. Comparing the B25 concrete to the results of the initial tests, there is a significant increase in compressive strength. The difference in compressive strength may be explained by the fact that it was not possible to store the beams in a heated water tank due to size of the beams. The beams and their cylinders were therefore stored in 20°C water instead of 42°C and the curing temperature may have influenced the final compressive strength. It is observed that the compressive strength of BC-50 is reduced compared to BC-REF, but is still larger than the compressive strength of C0-REF.

The slump for the beams is generally greater than the slump of the columns. However the sand used for the beams were damp than the sand used for the column. This is presumed to be the most significant cause for this difference. The dampness of the sand may also have influenced the differences in strength between the columns and beams. The same sand type were used for all the column recipes and a different sand type were used for all the beam recipes, therefore a consistent comparison can still be made within each group of tests.

2.6.3 Column test

A small difference is found in compressive strength between SC-REF and SC-25, which indicates that each individual casting may influence the final compressive strength a lot. However the difference is still small and some SC-REF cylinders have given weaker compressive strength results than some SC-25 cylinders. The SC-50 compressive strength is higher than the BC-50 and the C0-50 but still reduced significantly compared to SC-REF. This result indicates that is possible to obtain a relatively high compressive strength in the concrete even when replacing large amounts of cement with SSA.

The differences from the initial test to the beam and column concrete tests implies that differences in the concrete mixing process and curing process are highly important and can influence the final strength of concrete mix significantly.

2.7 Conclusion concrete

It is generally observed that the concrete strength will be affected when replacing cement with SSA, however in concentrations up to 25% SSA, the impact on the compressive strength is small. It is also observed that it is possible to make concrete with up to 50% SSA replacing cement and obtain a concrete with a reduced strength that however still fulfill the demands for structures in passive exposure class.

Based on the castings made, it is observed that the slump of the concrete will be affected when replacing cement with SSA. Generally a more dry and stiff concrete is obtained and this fact will have to be taken into account by the contractor or element producer intending to use SSA in his concrete recipes.

As the reduction in compressive strength for added SSA samples were smaller than expected, it gives an indication that SSA may have a puzzolanic properties, or at the very least filler abilities that can add compressive strength to the concrete in cooperation with cement.

3 Reinforcement steel

The reinforcement is supplied by Lemvigh-Müller in two shipments. Both shipments have a declared yield strength of 550 MPa according to DS/EN 10080:2006 and DS/INF 165:2009. The first shipment contains steel for one reinforcement cage used for B-REF-3 and is supplied from Denmark (DK). The second shipment contains steel for the remaining 17 cages and is supplied from Poland (PL). Both shipment includes rebar with diameters of 8 and 10 mm.

3.1 Theory

The relevant material properties of the reinforcement steel regarding this project are the Young's modulus (E) and the yield strength (f_y). The basis for the Young's modulus is Hooke's law for elastic materials where the force needed to elongate the material a distance is proportional to that distance. The proportionality factor called the Young's modulus is understood as the material stiffness. The exact relation is given:

$$\sigma = E \cdot \varepsilon \tag{3-1}$$

At large strains the material undergoes a transition to a plastic material phase where deformations remain permanent. This transition is called yielding. The experimental determination of the stiffness is defined in [13]. First the stress at 0.2% strain is determined $(\sigma_{p0.2})$. The stiffness is then made as a regression of the slope of the measured stresses and strains between 10% and 50% of $\sigma_{p0.2}$.

The yield stress is then determined by using the obtained E by imposing a linear line from the 0.2% strain with the slope E

$$\sigma_{y,det} = E \cdot \varepsilon - 0.002 \cdot E \tag{3-2}$$

The crossing between $\sigma_{y,det}$ and the working curve is then defined as the yield strength. This is the case for stress-strain curves without a visible yield plateau. For stress-strain curves with such a plateau the yield stress is determined as the average stress value for the plateau. Only the *PL 10 mm* has this visible yield plateau. The latter method of determination was discovered late in the post-processing and is not used in this project. Investigations show that the difference is insignificant. All other reinforcement bars used in the project however does not have a visible yield plateau and the first method is therefore used. An example is seen in Figure 3-1. Theoretically the material is regarded as ideal meaning it is linear-elastic until plasticity begins. In the plastic region, the material is considered stiff. This means the curved transition from linear-elastic to plastic is omitted. The theoretical definition of the material is seen in Figure 3-2.

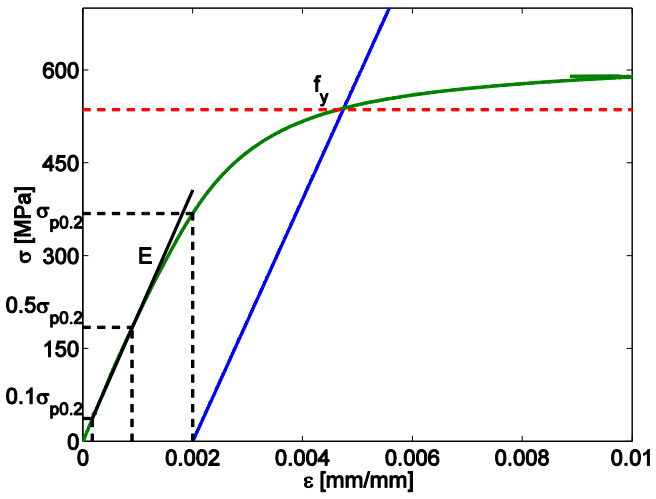

Figure 3-1: Practical determination of stiffness and yield stress of reinforcement test

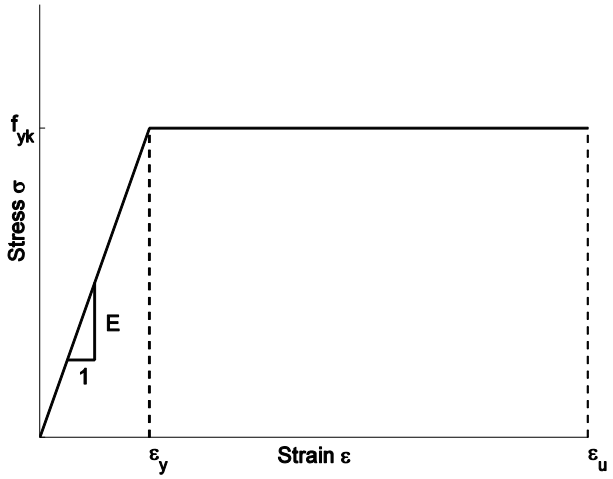

Figure 3-2: Theoretical definition of work curve for steel

3.2 Equipment and materials

- INSTRON 8502 100 kN universal testing machine
- INSTRON Strain Gauge Extensometer cat. No. 2630-116
- Data logger
- Metal band saw

3.3 Experimental description tensile test

1. Tensile test of reinforcement for determination of stiffness and yield strength.
2. The steel rebar is cut in length of 250 mm with a metal band saw.
3. The rod is placed in the tensile test machine.
4. The extensometer, with a gauge length of 50 mm is placed roughly at the middle of the rod.
5. The test consists of two different loading blocks.
6. The first block is used to determine the stiffness of the material. In this block the test machine has a piston displacement of 1.5 mm/min. When the material has reached strain of roughly 1%, the extensometer is removed from the rebar and the second block is initiated.
7. The second block is used to speed up the process of testing after yielding has started. A piston displacement of 20 mm/min is chosen.
8. When the ultimate strength of the rod has been reached the test is complete and the rod is removed from the test machine.
9. The data is extracted and post-processing is performed.

3.4 Results

The steel is delivered in two shipments due to an error at the supplier. Both shipments are tested, however as the DK shipment was not expected to be used only two 8 mm and two 10 mm were tested. The results are shown in Table 3-1. The mean values are used in the further calculations.

Table 3-1: Reinforcement yield strength and stiffness test results.

Shipment/diameter		1	2	3	4	5	Mean	Std. dev.
PL / 8 mm *	f_y $[MPa]$	560.8	559.1	–	562.0	541.0	**555.7**	9.9
	E [GPa]	204.3	177.8	–	158.7	181.6	**180.6**	18.7
PL / 10 mm**	f_y $[MPa]$	623.9	624.9	615.2	618.4	627.5	**622.0**	5.0
	E [GPa]	209.0	200.0	207.8	199.7	191.0	**201.5**	7.3
DK / 8 mm	f_y $[MPa]$	530.3	553.0	-	-	-	**541.6**	16.0
	E [GPa]	205.3	195.7	-	-	-	**200.5**	6.8
DK / 10 mm	f_y $[MPa]$	535.9	540.5	-	-	-	**538.2**	3.2
	E [GPa]	202.8	186.2	-	-	-	**194.5**	11.7

*The result in PL/8mm – 3 is omitted due to heavy signal noise in the early phase of the test.
**Hot-rolled steel with a yield plateau. All other bars are cold drawn.

3.5 Results evaluation

Looking at the standard deviation of the Young's Modulus E in Table 3-1 it is evident that the tests yield very different results. In the DK 10mm case only two rods are tested hence a statistical basis is not obtained – this counts for both diameters of the Danish delivery. For the PL 8mm case the obtained Young's modulus cannot be explained by other means than differences in the material compared to the other rebars. The mean E for the PL 8 mm (180.6 GPa) is observed lower than the rest of the samples ($194.5 - 201.5$) which is party caused by the 158.7 GPa sample.

Evaluating the yield stresses, the results are more consistent however not perfect. There is a significant difference between the hot-rolled and cold drawn steel. The cold drawn steel varies in the interval $[530.3\ ;\ 562.0]$ MPA with mean values between 538.2 and 555.7 MPa. The hot-rolled steel is very consistent in the interval $[615.2\ ;627.5]$ MPa with a mean of 622.0 MPa.

In all the cases the mean values are used for further calculations. To see the performance curves and determination of the yield strength and Young's modulus see appendix D.

4 Beam experiments

4.1 General thought on reinforcement design

In the design process it is determined to simplify the castings and the assembly of the reinforcement cages. To reducing the chances of mistakes the simplest possible solution is chosen. It is attempted to obtain the same amount of reinforcement in both top and bottom of the beams and columns and to use the same stirrups and spacing. The calculations show that the same reinforcement cages can be used for all beams and columns despite differences in concrete strength when replacing cement with SSA.

4.2 Calculation theory

Assumptions:

- Geometric condition: Plane cross sections remain plane. Meaning strain distribution is linear in cracked as well as uncracked situation.
- Physical condition: Reinforcement steel is considered ideal as shown in Figure 3-2. The compression zone is considered to have rectangular uniform stress in the height of the plastic part of the compression zone and completely cracked in the tension zone
- Static condition: The section forces are in equilibrium.
- The calculation takes all reinforcement into consideration.
- The experimentally determined material properties for reinforcement steel and concrete are used in the calculations. Mean values are used, and no partial coefficients are used.
- The actual dimensions of the beams are used in the calculations to eliminate tolerances.

4.2.1 Moment capacity

As a basis for the design of the reinforcement of the beam the preceding formulas and theory from [14] based on the method from [15].

The design of the beam reinforcement cage is made to fulfil the criteria of normal reinforcement for varying concrete strengths depending on the percentage of ash in the concrete. The criterion for normal reinforcement is given below.

$$\varepsilon_y \leq \varepsilon_s \leq \varepsilon_u \tag{4-1}$$

Where

ε_s is the strain in the steel when the concrete in compression fails
ε_y is the yield strain of the reinforcement steel
ε_u is the ultimate strain of the reinforcement steel

The equation states that the reinforcement steel should be yielding when the concrete fails, but not beyond failure in order to obtain a ductile behavior from the beam.

ε_s is calculated by solving six equations with six unknowns (4-2)-(4-7).

The strain in the tension steel

$$\varepsilon_s = \frac{\varepsilon_{cu3} \cdot (d - x)}{x} \tag{4-2}$$

The strain in the Compression steel

$$\varepsilon_{sc} = \frac{\varepsilon_{cu3} \cdot (d_c - x)}{x} \quad (4\text{-}3)$$

The stress in the tensile steel

$$\sigma_s = min\begin{bmatrix}\varepsilon_s \cdot E_s \\ f_{ym}\end{bmatrix} \quad (4\text{-}4)$$

The stress in the compression steel

$$\sigma_{sc} = min\begin{bmatrix}\varepsilon_{sc} \cdot E_s \\ f_{ym}\end{bmatrix} \quad (4\text{-}5)$$

Normal force equilibrium

$$N = 0 = \lambda \cdot x \cdot b \cdot f_{cm} + A_{sc} \cdot \sigma_{sc} - A_s \cdot \sigma_s \quad (4\text{-}6)$$

Moment equilibrium about middle

$$M = \lambda \cdot x \cdot b \cdot f_{cm} - \left(\frac{h}{2} - \frac{\lambda \cdot x}{2}\right) + A_{sc} \cdot \sigma_s - A_s \cdot \sigma_s - A_{sc} \cdot \sigma_{sc} \cdot \left(\frac{h}{2} - d_c\right) + A_s \cdot \sigma_s \cdot \left(d - \frac{h}{2}\right) \quad (4\text{-}7)$$

Where:

M	Moment
N	Normal force
x	height of the elastic compression zone
d	effective height of the cross section
d_c	distance form the reinforcement in compressiomn to the top of the compression zone
ε_{cu3}	ultimate strain of the concrete with bending
λ	a factor for distributing the compression stresses in the concrete by plasticity. $\lambda = 0.8$ for rectangular cross sections
A_s	area of the reinforcement in tension
A_{sc}	area of reinforcement in compression
h	height of the cross section
f_{cm}	mean compressive strength of the concrete
f_{ym}	mean yield stress of the reinforcement
σ_s	stresses in the tensile reinforcement
σ_{sc}	stresses in the compression reinforcement
ε_s	strain in the tensile reinforcement
ε_{sc}	strain in the compression reinforcement

The equations are solved for the unknowns M, x, ε_s and ε_{sc} and the stresses σ_s and σ_{sc} that depends on the strains in the steel and the yield stress of the steel. To optimize the calculations an excel sheet have been used where an iterative approach have been applied to find the height of the compression zone with equilibrium of the normal-forces that are equal to zero for pure bending. The solver function in excel have been used.

The general dimensions of the beams are 125x250mm with a length of 2200 mm. For these dimensions, different diameters of reinforcement steel have been tested by trial and error with the assumption that the compressive strength of the concrete might go all the way down to 10 MPa[1], when the maximum amount of ash is applied. The chosen reinforcement diameters are shown in Figure 4-1. In order to ensure complete anchoring two U-shaped Ø10 bars are placed at each end of the beam.

[1] The calculations have been made before the initial cylinders have been tested, which is the reason for the assumption

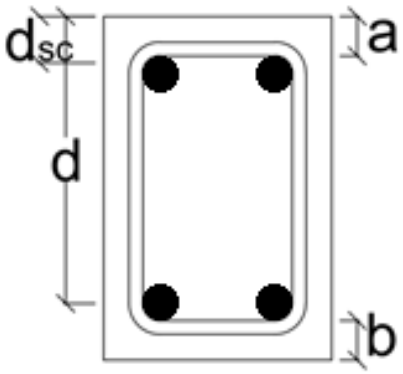

The longitudinal reinforcement: 2 Ø10 bars in top and bottom
Shear reinforcement: Ø8 with c/c distance of 100 mm

Figure 4-1: Geometry of cross section

The detailed beam calculation results can be found in appendix E.

4.2.2 Shear capacity

In the experiments the moment capacities are primarily investigated and the shear reinforcement is therefore designed to ensure bending failure. The stirrups are therefore placed with a small distance to ensure the shear capacity of the beams. Earlier investigations [16] have shown that placing the stirrups to close together will influence the moment capacity due to confinement of the concrete. The distance is therefore set to 100mm for most of the beam. In the outermost 300 mm of the beams the stirrups are placed with 50mm spacing instead, as the shear forces are dominating in this part of the beam. Furthermore, the calculations show that the abutment in the experiment is too small to allow full anchoring of the longitudinal reinforcement, which is why U-stirrups are placed in the ends to obtain full anchoring.

The shear capacity is calculated by equations (4-8)-(4-13).

Number of stirrups going through a stringer

$$n_w = z \cdot \frac{\cot(\theta)}{s} \tag{4-8}$$

Shear capacity stirrups

$$V_{r.w} = n_w \cdot A_{sw} \cdot f_y \tag{4-9}$$

Shear capacity longitudinal reinforcement

$$V_{r.l} = \frac{2 \cdot f_y \cdot A_s}{\cot(\theta)} \tag{4-10}$$

Effectivity factor

$$\nu_\nu = 0.7 - \frac{f_{cm}}{200MPa} \tag{4-11}$$

Shear capacity concrete stringer

$$V_{r.c} = \frac{\nu_\nu \cdot f_{cm} \cdot w \cdot z \cdot \cot(\theta)}{1 + \cot(\theta)^2} \tag{4-12}$$

Shear capacity beam

$$\mathrm{V_r} = \min(V_{r.c} \quad V_{r.l} \quad V_{r.w}) \tag{4-13}$$

Where:

z	internal moment arm
θ	angle of concrete compressive stringer
s	distance between stirrups
A_{sw}	cross section area of stirrups
w	width of cross section

The angle of the concrete stringer θ has been optimized to obtain the maximum shear capacity possible which is approximately $\theta = 37°$ resulting in $\cot(\theta) = 1.3$. Based on the calculations the stirrup diameter is chosen to be 8mm and have a spacing of 100mm. This yields a shear capacity of approximately 150kN which is approximately 3.5 times the necessary shear capacity for the beam as the maximum loads applied is approximately 42kN. Since the reinforcement design is identical for the beams and columns, the stirrup distance at the supports is decreased to 50mm to ensure shear capacity and avoid local crushing in the columns.

4.2.3 Theoretical curvature

The theoretical curvature of the beam is calculated in order to have a frame of reference for the beam behavior. The theoretical curvature is based on elastic behavior and can therefore only be compared to the experiments on parts of the moment-curvature plot.

The theoretical curvature is determined by calculating the displacement at the middle for two cases of simply supported beams. A single load is placed as either of the loads in the experiment. The principle of superposition is applied to obtain the theoretical displacement for the beam in the experiment.

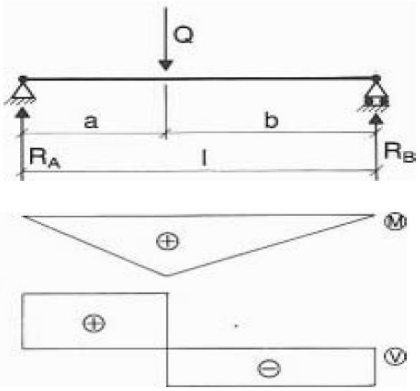

Figure 4-2: displacement for a simple supported beam with a single load placed arbitrarily on the beam. [17]

The displacement is calculated for each beam using the following equations:

$$u(x) = \frac{1}{6} \cdot \frac{Q \cdot b \cdot l \cdot x}{E \cdot I} \cdot \left(1 - \left(\frac{b}{l}\right)^2 - \left(\frac{x}{l}\right)^2\right) \; for \; x \leq a \tag{4-14}$$

$$u(x) = \frac{1}{6} \cdot \frac{Q \cdot a \cdot l \cdot (l - x)}{E \cdot I} \cdot \left(\frac{2 \cdot x}{l} - \left(\frac{a}{l}\right)^2 - \left(\frac{x}{l}\right)^2\right) \; for \; x \geq a \tag{4-15}$$

The measured dimensions and material properties for the beams are used as a basis for the calculations.

4.2.4 Maximum theoretical crack distance

The cracks are not important in relation to the carrying capacity. The cracks are in a way necessary to activate the tension reinforcement, however the durability of the beam will decrease as cracks leads to ingress of water to the reinforcement steel. Presence of water is a necessity for the corrosion process to happen. The size of the cracks is dependent on the distance between the cracks, where a big distance will lead to fewer but wider cracks. A small distance between the cracks is preferable.

The max distance between the cracks is calculated as:

$$S_{r,max} = 29 \cdot \sqrt[3]{c} + 0.17 \cdot \frac{w \cdot h_{c,eff}}{A_s} \cdot Ø \quad (4\text{-}16)$$

Where:

$$h_{c,eff} = \min\left(\frac{5}{2} \cdot (h - d); \frac{h - x}{3}; \frac{h}{2}\right) \quad (4\text{-}17)$$

To be able to use (4-16) the distance between the tension reinforcement should fulfil:

$$S_Ø \leq 5 \cdot \left(c + \frac{Ø}{2}\right) \quad (4\text{-}18)$$

4.3 Results of theoretical calculations

The results of the theoretical beam calculations are presented in Table 4-1.

Table 4-1: Theoretical calculation results for beams

Beam No.	Moment capacity M_R [kNm]	Compression zone height X [mm]	Tensile Steel strain ε_s [%]	Shear capacity V_R [kN]	Maximum crack distance s_{max} [mm]
B-REF-1	20.8	28.2	2.35%	149.9	191.19
B-REF-2	20.6	25.8	2.60%	150.6	195.69
B-REF-3	20.4	26.4	2.50%	149.6	196.92
B-25-1	20.7	26.4	2.56%	151.0	190.21
B-25-2	20.8	26.1	2.60%	152.0	195.10
B-25-3	20.5	26.1	2.56%	150.8	194.38
B-50-1	19.9	35.8	1.81%	148.6	187.78
B-50-2	19.7	36.2	1.77%	147.9	191.07
B-50-3[2]	16.4	34.0	1.81%	133.4	194.80

It is determined that all the beams will obtain ductile failure mechanisms as the strain in the reinforcement will result in 5.3-8.4 times the yield strain. Based on the calculations it is observed that the reduction in concrete compressive strength does not influence the moment bearing capacity of the beams significantly as the reduction is only about 5% for the B-50 series (except for B-50-3, that have different reinforcement)

[2] This beam is the only beam with different reinforcement than the rest of the beams. (using Danish reinforcement)

4.4 Sensitivity analysis of beam calculations

A sensitivity analysis has been conducted in order to obtain knowledge on the precision of the beam calculations and how they are affected by uncertainties in the parameters of the beams. The parameters examined are:

- The compressive strength of the concrete (f_c)
- The concrete fracture strain (ε_{cu3})
- The yield stress of the longitudinal reinforcement (f_{yl})
- The Young's modulus of the longitudinal reinforcement (E_s)
- The depth of the reinforcement in the tension zone (d)
- All of the above combined

The calculations are performed for mean values and limits of the 95% confidence interval defined in (4-19). These values are found by performing test on the concrete and the reinforcement steel.

$$\begin{cases} 1.645 \cdot \sigma - \mu \\ \mu \\ 1.645 \cdot \sigma + \mu \end{cases} \tag{4-19}$$

Where

μ	Mean value of the analyzed parameter
σ	Standard deviation of the analyzed parameter

The parameter intervals are used to examine the effect on the following results of the beam calculations.

- The moment capacity (M_{Rm})
- The Shear capacity (V_{Rm})
- The strain of the longitudinal reinforcement in tension (ε_{st})
- The maximum length theoretical distance between the cracks ($s_{r,max}$)

The Maple-scripts used for the calculations can be found in appendix F.

4.4.1 Concrete compressive strength

The compressive strength of the concrete is determined by casting cylinders of concrete from the same batch as the concrete used for the beams. The cylinders are tested and a mean and standard deviation are calculated. These are converted into an upper and a lower value, which are shown alongside the results of the analysis in Table 4-2.

Table 4-2: Results of sensitivity analysis for variations in concrete strength

Concrete - compressive strength					
		M_R	ε_{st}	V_R	$s_{r,max}$
		[kNm]	[-]	[kN]	[mm]
Reference concrete	f_c = 39.8 MPa	20.5	0.0237	150.3	89.3
	f_c = 43.8 MPa	20.7	0.0250	150.3	89.3
	f_c = 47.9 MPa	20.9	0.0262	150.3	89.3
	Diff. lower	0.87 %	5.09 %	0.00 %	0.00 %
	Diff. upper	0.83 %	4.86 %	0.00 %	0.00 %
Concrete with 25 % SSA	f_c = 39.7 MPa	20.5	0.0245	150.3	87.5
	f_c = 43.3 MPa	20.7	0.0257	150.3	87.5
	f_c = 47.0 MPa	20.8	0.0268	150.3	87.5
	Diff. lower	0.73 %	4.65 %	0.00 %	0.00 %
	Diff. upper	0.70 %	4.46 %	0.00 %	0.00 %
Concrete with 50 % SSA	f_c = 15.8 MPa	19.1	0.0149	114.9	86.3
	f_c = 20.8 MPa	19.4	0.0174	138.0	86.3
	f_c = 25.7 MPa	19.6	0.0196	138.0	86.3
	Diff. lower	1.44 %	14.19 %	16.73 %	0.00 %
	Diff. upper	1.30 %	12.57 %	0.00 %	0.00 %

From Table 4-2 it is seen that the moment capacity is not affected significantly by the change in concrete strength. The concrete strength has a relatively large effect on the strain of the steel. As both the upper and lower value of the strain are inside the limits for the normal reinforced beams it is considered acceptable. The shear capacity is only affected for the B-50 series, since the shear capacity is over dimensioned it is still acceptable. The maximum theoretical crack distance is not affected at all.

4.4.2 The concrete fracture strain

The fracture strain of the concrete is not determined experimentally and is assumed constant, hence there is no mean or standard deviation to use for the analysis. The upper and lower values of the fracture strain have therefore been chosen as 3 ‰ and 4 ‰ respectively. The results are shown in Table 4-3.

Table 4-3: Results of sensitivity analysis with respect to the concrete fracture strain

Concrete - fracture strain					
		M_R	ε_{st}	V_R	$s_{r,max}$
		[kNm]	[-]	[kN]	[mm]
Reference concrete	$\varepsilon_{cu,3}$ = 3.0 ‰	20.7	0.0217	150.3	89.3
	$\varepsilon_{cu,3}$ = 3.5 ‰	20.7	0.0250	150.3	89.3
	$\varepsilon_{cu,3}$ = 4.0 ‰	20.7	0.0282	150.3	89.3
	Diff. lower	0.08 %	13.03 %	0.00 %	0.00 %
	Diff upper	0.06 %	12.87 %	0.00 %	0.00 %
Concrete with 25 % SSA	$\varepsilon_{cu,3}$ = 3.0 ‰	20.7	0.0223	150.3	87.5
	$\varepsilon_{cu,3}$ = 3.5 ‰	20.7	0.0257	150.3	87.5
	$\varepsilon_{cu,3}$ = 4.0 ‰	20.7	0.0291	150.3	87.5
	Diff. lower	0.05 %	13.24 %	0.00 %	0.00 %
	Diff. upper	0.05 %	13.10 %	0.00 %	0.00 %
Concrete with 50 % SSA	$\varepsilon_{cu,3}$ = 3.0 ‰	19.4	0.0145	138.0	86.3
	$\varepsilon_{cu,3}$ = 3.5 ‰	19.4	0.0174	138.0	86.3
	$\varepsilon_{cu,3}$ = 4.0 ‰	19.4	0.0203	138.0	86.3
	Diff. lower	0.00 %	16.40 %	0.00 %	0.00 %
	Diff. upper	0.00 %	16.75 %	0.00 %	0.00 %

From Table 4-3 it is seen that the variation in the fracture strain has little or no effect on the moment capacity, shear capacity or the maximum crack distance. The steel strain is affected, however as for the concrete strength the beams are still normal reinforced, which is acceptable.

4.4.3 Yield stress of the reinforcement

The yield stress of the longitudinal reinforcement is determined by performing tensile tests on the steel and calculating the mean and standard deviation of the sample. The upper and lower values and the results of the sensitivity analysis are shown Table 4-4.

Table 4-4: Results of the sensitivity analysis with respect to the yield stress of steel

Longitudinal reinforcement - yield stress					
		M_R	ε_{st}	V_R	$s_{r,max}$
		[kNm]	[-]	[kN]	[mm]
Reference concrete	f_y = 613.7 MPa	20.5	0.0252	148.3	89.3
	f_y = 622.0 MPa	20.7	0.0250	150.3	89.3
	f_y = 630.3 MPa	21.0	0.0249	150.9	89.3
	Diff. lower	1.20 %	0.59 %	1.33 %	0.00 %
	Diff. upper	1.20 %	0.59 %	0.37 %	0.00 %
Concrete with 25 % SSA	f_y = 613.7 MPa	20.4	0.0259	148.3	87.5
	f_y = 622.0 MPa	20.7	0.0257	150.3	87.5
	f_y = 630.3 MPa	21.0	0.0255	151.5	87.5
	Diff. lower	1.21 %	0.61 %	1.33 %	0.00 %
	Diff. upper	1.21 %	0.61 %	0.77 %	0.00 %
Concrete with 50 % SSA	f_y = 613.7 MPa	19.1	0.0175	138.0	86.3
	f_y = 622.0 MPa	19.4	0.0174	136.1	86.3
	f_y = 630.3 MPa	19.6	0.0172	136.1	86.3
	Diff. lower	1.25 %	0.95 %	1.35 %	0.00 %
	Diff. upper	1.25 %	0.94 %	0.00 %	0.00 %

From Table 4-4 it is observed that the resulting parameters are not significantly affected due to the low variation in the yield stress.

4.4.4 Young's modulus of the reinforcement

The Young's modulus is measured while conducting the tensile test on the reinforcement. On the basis of this the lower and upper values are shown in Table 4-5.

Table 4-5: Results of the sensitivity analysis with respect to the Young's modulus of the reinforcement

Longitudinal reinforcement - Young's Modulus					
		M_R	ε_{st}	V_R	$s_{r,max}$
		[kNm]	[-]	[kN]	[mm]
Reference Concrete	E_s = 189 GPa	20.7	0.0251	150.3	89.3
	E_s = 201 GPa	20.7	0.0250	150.3	89.3
	E_s = 214 GPa	20.7	0.0249	150.3	89.3
	Diff. lower	0.03 %	0.58 %	0.00 %	0.00 %
	Diff. upper	0.03 %	0.54 %	0.00 %	0.00 %
Concrete with 25 % SSA	E_s = 189 GPa	20.7	0.0258	150.3	87.5
	E_s = 201 GPa	20.7	0.0257	150.3	87.5
	E_s = 214 GPa	20.7	0.0256	150.3	87.5
	Diff. lower	0.02 %	0.48 %	0.00 %	0.00 %
	Diff. upper	0.02 %	0.45 %	0.00 %	0.00 %
Concrete with 50 % SSA	E_s = 189 GPa	19.4	0.0172	138.0	86.3
	E_s = 201 GPa	19.4	0.0174	138.0	86.3
	E_s = 214 GPa	19.4	0.0175	138.0	86.3
	Diff. lower	0.00 %	0.99 %	0.00 %	0.00 %
	Diff. upper	0.00 %	0.94 %	0.00 %	0.00 %

From Table 4-5 it is observed that as for the yield stress of the reinforcement the standard deviations are small which mean that varying it has a small or no effect on the resulting parameters.

4.4.5 Depth of the tension reinforcement

The depth of the tensile reinforcement is determined by breaking open the beams after the bending tests and measuring it. The upper and lower values of the depths are shown in Table 4-6.

Table 4-6: Results of the sensitivity analysis with respect to the depth of the reinforcement

Depth of longitudinal reinforcement					
		M_R	ε_{st}	V_R	$s_{r,max}$
		[kNm]	[-]	[kN]	[mm]
Reference concrete	d = 216.1 mm	20.5	0.0247	149.2	94.2
	d = 218.4 mm	20.7	0.0250	150.3	89.3
	d = 220.7 mm	20.9	0.0253	150.3	83.8
	Diff. lower	1.09 %	1.20 %	0.72 %	5.46 %
	Diff. upper	1.09 %	1.20 %	0.00 %	6.10 %
Concrete with 25 % SSA	d = 216.4 mm	20.4	0.0254	149.6	88.2
	d = 219.0 mm	20.7	0.0257	150.3	87.5
	d = 221.6 mm	21.0	0.0261	150.3	86.7
	Diff. lower	1.24 %	1.37 %	0.48 %	0.84 %
	Diff. upper	1.24 %	1.37 %	0.00 %	0.85 %
Concrete with 50 % SSA	d = 206.0 mm	18.4	0.0164	138.0	88.0
	d = 216.0 mm	19.4	0.0174	138.0	86.3
	d = 226.0 mm	20.3	0.0183	138.0	84.7
	Diff. lower	5.06 %	5.58 %	0.00 %	1.92 %
	Diff. upper	5.06 %	5.58 %	0.00 %	1.94 %

From Table 4-6 it is observed that the depth of the reinforcement has a considerable effect on the parameters except for the shear capacity. The large standard deviation of d in the reference concrete is responsible for the large variation in the maximum crack distance.

4.4.6 All parameters combined

To investigate the combination of all the described parameters the analysis is made with variation on all the parameters combined. The results of this are shown in Table 4-7.

Table 4-7: Sensitivity analysis with all parameters varying

All parameters at the same time					
		M_{Rd}	ε_{st}	V_{Rd}	$s_{r,max}$
		[kNm]	[-]	[kN]	[mm]
Reference concrete	Lower values	20.1	0.0205	148.3	94.2
	Mean values	20.7	0.0250	150.3	89.3
	Upper values	21.4	0.0295	152.3	83.8
	Diff. lower	3.21 %	17.82 %	1.33 %	5.46 %
	Diff. upper	3.26 %	18.07 %	1.33 %	6.10 %
Concrete with 25 % SSA	Lower values	20.0	0.0211	148.3	88.2
	Mean values	20.7	0.0257	150.3	87.5
	Upper values	21.4	0.0304	152.3	86.7
	Diff. lower	3.22 %	17.81 %	1.33 %	0.84 %
	Diff. upper	3.27 %	18.16 %	1.33 %	0.85 %
Concrete with 50 % SSA	Lower values	17.9	0.0115	114.9	88.0
	Mean values	19.4	0.0174	136.1	86.3
	Upper values	20.9	0.0238	136.1	84.7
	Diff. lower	7.74 %	33.99 %	15.61 %	1.92 %
	Diff. upper	7.67 %	36.80 %	0.00 %	1.94 %

From Table 4-7 it is observed that the deviations become quite considerable when all the deviations of the parameters are combined. The strains in the reinforcement have large deviations, but both the upper and lower results are within the limits for a normal reinforced beam. The moment and shear capacities and the crack distances have allowable deviations.

4.4.7 Result evaluation sensitivity analysis

Based on the sensitivity analysis described in this chapter it is concluded that there are insecurities in the parameters used in the beam calculations. The insecurities are covered and it is shown that these do not change the assumption that the beams are normal reinforced. Also it is unlikely that all the parameters have a "worst case" deviation. Should this occur it is proven that the deviations in the theoretical calculation are small. The sensitivity analysis shows that the calculations are acceptable.

4.5 Beam Production

The design of the beam is determined by the size of the available molds shown in Figure 4-3. The inner dimensions are 125x250x2200mm. The reinforcement design is determined based on the expected material strengths for the reinforcements and the different concrete types. The reinforcement is designed so that the beams (and columns) will fulfill the condition of a normal reinforced cross section. The expected yield stress of the reinforcement steel is in the interval 600-800 MPa, and the compression strength of the concrete is in the interval 10-40 MPa.

Figure 4-3: Beam and column molds, with reinforcement cages.

4.5.1 Equipment reinforcement assembly

- Tie tools
- Rebar ties.
- Rebars Ø10 and stirrups Ø8 and U-stirrups Ø10

4.5.2 Reinforcement assembly

1. The lower two longitudinal reinforcement bars is connected with at least 10 of the stirrups using rebar ties that is twisted around the reinforcement bars using the tie tools.
2. The upper two longitudinal reinforcement bars is then connected with the reinforcement cage.
3. The rest of the stirrups are connected to the cage, with the two lifting stirrups in the correct position.
4. The U-stirrups is inserted in the ends of the beams and connected to the longitudinal reinforcement.

4.5.3 Equipment and materials casting of beams

- Slump test equipment (cone, rod, and flat steel surface)
- Buckets to measure components into
- Buckets with closed lids for SSA
- Electric whisk for suspending SSA in water
- Shear force concrete mixer (200 L)
- Shovels.
- Wheelbarrows
- Rod vibrator
- Five Cylinder molds for each concrete type, with lids and clamps
- Three beam molds for each concrete type
- Plastic to cover the molds
- Curing basin
- Pallets and pallet lifter
- Scale for measuring the materials on
- Reinforcement cages and plastic spacers

4.5.4 Casting and curing of beams

1. The reinforcement cages are placed in the molds using plastic spacers to obtain the desired cover of 15mm in both top, bottom and sides.
2. The raw materials are measured by weight, into separate containers. The composition is shown in appendix B.
3. The SSA is measured out into buckets with a closeable lid in no larger amounts than 10 kg at a time. Part of the water is then carefully poured into the SSA to suspend the SSA particles and prevent the SSA from giving of dust.
4. The dry materials is then poured into the concrete mixer and mixed for 300 sec.
5. The super plasticizer is poured into the concrete mixer.
6. For the reference mix the water is poured in and the concrete is mixed for another 300 sec. for the other concrete mixes the suspended SSA is poured in and the bucket is rinsed with the rest of the mixing water which then is poured into the mixer, and the mixer is run for another 300 sec.
7. A slump test is performed in accordance with [11] for both reference and SSA mixes.
8. The concrete mixer is emptied into wheelbarrows and the concrete is put into the molds using shovels.
9. The concrete is vibrated to fill out the molds and enclose the reinforcement. The vibration is performed with a rod vibrator until it is estimated that the concrete fills out the form and encloses the reinforcement sufficiently, and no large air void is left.
10. Step 7 and 8 is repeated until a mold is filled with concrete, and the surface is smoothed using a brick trowel.
11. Along with the beams 5 cylinders are also cast according to the description specified in section 2.4.
12. After 24 hours the beams are de-molded and placed in a basin with water along with the cylinders. The water is at room temperature (20°C).
13. After 3 weeks the beams are removed from the basin and are ready to be tested.

4.6 Experimental description bending experiments

4.6.1 Initial setup

When the beams reach the desired maturity, the bending tests are carried out to determine the moment capacity. The test setup is a bending machine specifically designed for experiments with transversal loading. The static system is a four point bending setup of a simply supported beam as shown in Figure 4-4. The positions of the loads and the supports are defined by the user. The values are approximated the values shown in the static system.

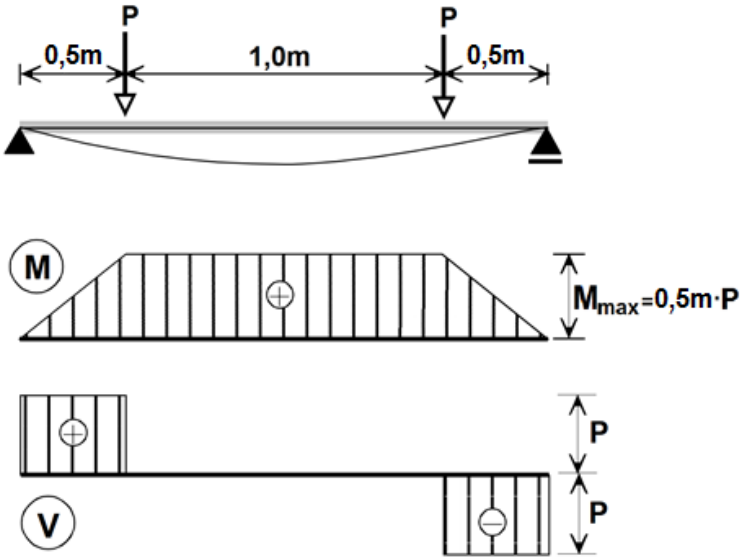

Figure 4-4: Static system for four point bending of a simple supported beam

The bending machine is shown in Figure 4-5. The setup is upside-down to what would be expected from a simply supported beam. The load direction is upwards and the reactions at the supports are directed downwards. This does not change the behavior of the beam as the reinforcement in the top and bottom of the beam is the same. The displacements of the beam are measured with electronic extensometers that are mounted on the upper steel beam of the machine using magnetic stands with hydraulic arms.

Figure 4-5: General view of the beam testing setup.

Figure 4-6: Extensometers

4.6.2 Equipment list for bending experiments

- Bending machine consisting of:
    - Control console for hydraulic pump
    - Hydraulic pump and oil tank
    - Hydraulic hoses to in- and outlet flow of oil.
    - Load pistons with a diameter of 95mm.
    - Load transfer steel blocks
    - Load distributing hard wood blocks
    - Support frames
    - Oil transducer to measure oil pressure
- electronic displacement gauges
- 11 magnetic stands with hydraulic arms
- cables to connect displacement gauges and oil transducer
- Crane with hooked chains
- Video cameras (1 regular, 1 with fish eye lens)
- Data logging station
- Permanent markers, measure tape and ruler

4.6.3 Four point bending testing

1. The supports are adjusted in relation to the load points to obtain the desired distances between the loads and supports. The distance between the load points is fixed, but the supports are moveable and are adjusted accordingly. The desired distances are shown in Figure 4-4.
2. The beam is placed in the test apparatus and centered using the crane. The setup is made so the tensile reinforcement will be in the top of the beam and the compression zone in the bottom. The loads will be applied upwards.
3. The hardwood blocks are placed between the steel load transfer blocks on the pistons and the beam to avoid local fractures at the load points.
4. Oil pressure is applied on the pistons to lift the beam off the temporary supports to fine adjust the position of the beam before lifting it onto the supports and a small load (max 3 kN) is seen on the dial gauge on the load machine.
5. The beam is marked at the supports, load points and at the center.
6. The seven electronic extensometers (Figure 4-6) are mounted with the magnetic holders on the steel beam situated on top of the test apparatus. The extensometers are adjusted and positioned on the beam at the marks of the center and load points of the beam, as well as on each side of the supports. The extensometers on each side of the supports are used to measure any displacement of the supports. The extensometers on the middle and the load points are used to calculate the curvature of the beam during loading.
7. The precise position of the marks are measured, noted and used in the post-processing of the data.
8. The data-logger and cords are tested and started simultaneously.
9. The test is carried out with the control panel on setting II allowing a maximum load from each piston of 100kN. The load rate is approximately 2 kN/min. The load speed is regulated manually, why it is approximated.
10. The test is complete when there are cracks in the concrete at the top, compression failure at the bottom and the load has reached its maximum.
11. The pistons are retracted and the steel beam with the seven extensometers is moved to the side.
12. The beam is removed from the test setup.
13. The crack pattern is marked and the distance between the cracks is measured.
14. The covering layer is removed with a hammer and a chisel. The cover thickness to the longitudinal reinforcement on both the compression and tension side is measured.

4.7 Post processing of logged data, bending tests

4.7.1 Oil pressure

The bending machine applies load to the beam by increasing the oil pressure on the pistons. This oil pressure is registered with an oil transducer as a voltage signal registered in the data-logger. The oil pressure in MPa is calculated from voltage signal as:

$$p = \frac{(U - 0.000124) \cdot 4928821}{1000} \tag{4-20}$$

4.7.2 Load

The oil pressure is converted to a load by pressing on the piston surfaces in the oil circuit. This pressure is transferred to the beam with a force equal to the oil pressure times surface area of the pistons:

$$F = p \cdot A_{piston} \tag{4-21}$$

4.7.3 Moment

As four point bending is used the maximum moment will be constant between the two applied loads. The moment will be calculated as:

$$M = F \cdot a \tag{4-22}$$

4.7.4 Displacement

The displacement is registered in electronic extensometer were a needle is displaceable by 100mm, which is registered in the extensometer as a change in voltage. The voltage varies from 0 to 5 volts over the 100 mm displacement of the needle.

$$\Delta s = \Delta U \cdot \left(\frac{100mm}{5V}\right) \tag{4-23}$$

4.7.5 Compensation for displacements of supports

Compensation for the displacements of the support point is performed to ensure that the actual deformation of the beam is obtained from the measured displacements. The extensometers placed on each side of the supports registers the movement of the supports as shown in Figure 4-7.

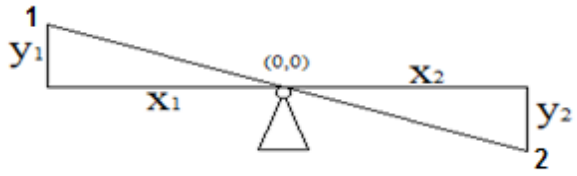

Figure 4-7: Displacement of support by measuring the displacement on each side of the support.

For each logging the displacement in each of the two extensometers are registered as y_1 and y_2 and the distance they are placed from the supports as x_1 and x_2. The displacement y_3 in the support can then be calculated as:

$$y_3 = y_2 - \frac{y_2 - y_1}{x_2 - x_1} \cdot x_2 \tag{4-24}$$

The obtained displacements of the supports can be used to obtain the actual displacements at the load points and the midpoint of the beam. The compensation takes the distance from each support into consideration to obtain the most accurate displacement in each measuring point. The geometrical principle is shown in Figure 4-8.

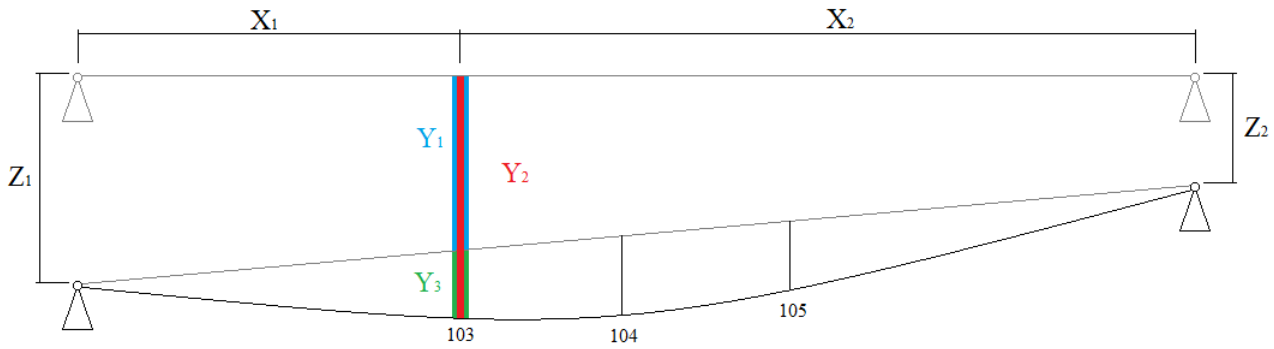

Figure 4-8: Adjustments of the measured displacement Y_2 in a measuring point based on displacements Z_1 and Z_2 in the supports to obtain the actual displacement Y_3

The actual displacement of the measuring points is calculated as:

$$Y_3 = Y_2 - \left(Z_1 + \frac{X_1}{X_1 + X_2} \cdot (Z_2 - Z_1) \right) \tag{4-25}$$

4.7.6 Curvature beams

The curvature describes the change of an angle of a tangent as a function of the traveled arch length:

$$\kappa = \frac{\Delta\alpha}{L_{arch}} = \frac{1}{r} \tag{4-26}$$

The curvature is constant for a beam with a constant moment. This is the case between the load points of the beam in the four point bending experiment. The derivation of the curvature is performed in (4-27)-(4-29).

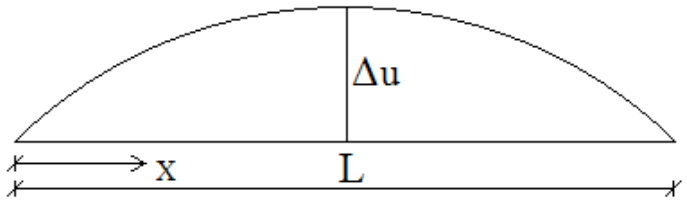

Figure 4-9: Displacement field for the part of the beam with a constant moment.

The displacement field for Figure 4-9 is derived as:

$$w = K \cdot \left(\frac{x}{L}\right) \cdot \left(1 - \frac{x}{L}\right) \tag{4-27}$$

The factor K can be found for $x = \frac{L}{2}$ where we know the displacement is equal to Δu

$$\Delta U = K \cdot \left(\frac{1}{2}\right) \cdot \left(1 - \frac{1}{2}\right) \rightarrow K = 4\Delta u \tag{4-28}$$

When the displacement field is differentiated with respect to x twice, the equation for the curvature is obtained

$$\kappa = \frac{d^2}{dx^2}\left(4\Delta u \cdot \left(\frac{x}{L}\right) \cdot \left(1 - \frac{x}{L}\right)\right) = -\frac{8\Delta u}{L^2} \tag{4-29}$$

In the experiments the displacement are measured on the whole beam but the moment is only constant between the load point why the displacement in relation to the zero-line going through these two point must be found as shown in Figure 4-10. The length between the two load points $a = L$ in (4-29).

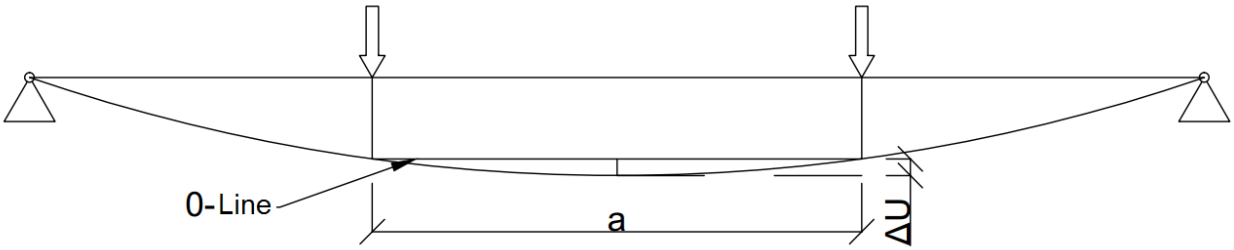

Figure 4-10: Basis for calculation of curvature.

4.7.7 Curve radius

To better understand the curvature, the curve radius is calculated as the inverse value of the curvature.

$$r = \frac{1}{\kappa} \tag{4-30}$$

4.8 Moment-curvature relation

The moment-curvature relation compares the obtained moment in the beam with the appertaining curvature to understand the change of the relation of the bending behavior of the beams. For a linear elastic isotropic beam, the relation between the moment and the curvature will be constant. For a reinforced concrete beam, the relationship changes as the concrete cracks due to its low tensile strength and the reinforcement yields. The ideal moment-curvature relation is shown in Figure 4-11.

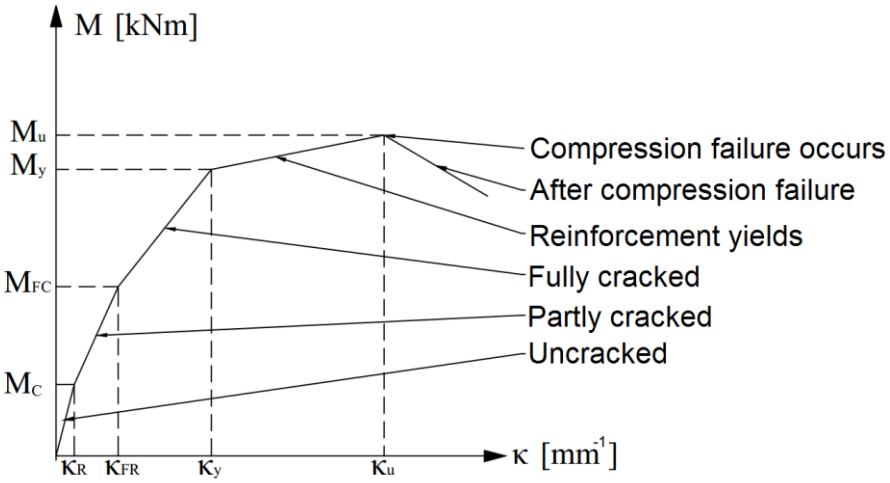

Figure 4-11 Theoretical moment-curvature relationship in a normal reinforced concrete beam

In the beginning of the experiment the beam is completely intact and the tensile strength of the concrete adds to the bending stiffness of the beam resulting in a very steep slope of the moment-curvature relationship. The concrete begins to crack in the tension zone of the beam when the tensile strength of the concrete is exceeded. The slope of the moment curvature relationship then decreases until a fully cracked cross section is obtained. When the reinforcement begins to yield the slope decreases further. After yielding of the reinforcement only a small increase in the moment capacity is observed, which originates from the strain hardening of the reinforcement. The theoretically calculated moment capacity cannot take the strain hardening into account as the reinforcement is assumed ideal.

4.9 Experimental results and discussion four point beam bending experiments

In this subsection the results of the four point bending experiment are presented. The detailed results of each individual beam is presented appendix G.

4.9.1 Experimental moment capacity and comparison to theoretical values

Table 4-8: Experimental results for beam experiments

Beam	Moment capacity (M_{u2}) $[kNm]$	Mean moment capacity ($\overline{M_{u2}}$) $[kNm]$	Theoretical moment capacity (M_r) $[kNm]$	$\frac{M_{u2}}{M_r}$	$\frac{\overline{M_{u2,REF}}}{\overline{M_{u2}}}$
B-REF-1	21.5		20.8	103.41%	
B-REF-2	21.4	21.4	20.6	104.11%	100%
B-REF-3	21.4		20.4	105.05%	
B-25-1	21.6		20.7	103.99%	
B-25-2	21.3	21.2	20.8	102.15%	99.1%
B-25-3	20.7		20.5	100.95%	
B-50-1	20.5		19.9	102.92%	
B-50-2	20.4	20.4	19.7	103.80%	95.3%
B-50-3	20.4		16.4	124.51%	

It is observed that the moment capacities obtained in the experiments are very close to the theoretical values, and varies less than 5 %, which is a satisfying result. This is validated by the sensitivity analysis yielding deviations from 0 % to 7.5 % depending on parameter varied shown in section 4.4. The only result deviating a lot is the theoretical results of B-50-03 which used Danish reinforcement steel with a lower yield stress than the Polish steel used in the rest of beams (and columns). This lower yield strength have influenced the theoretical moment capacity of the beams significantly, but for unexplainable reasons the bending experiment of B-50-03 yield a very similar moment capacity compared to B-50-02 and B-50-01. One suggested explanation is an increase in stresses of the reinforcement after yield caused by strain hardening of the reinforcement. Alternatively human or measurement errors in the tensile experiments of the Danish reinforcement may have occurred leading to lower measured yield strength than actually occurring.

4.9.2 Moment-curvature relationship

The moment-curvature relations for the beam experiments are presented in Figure 4-12.

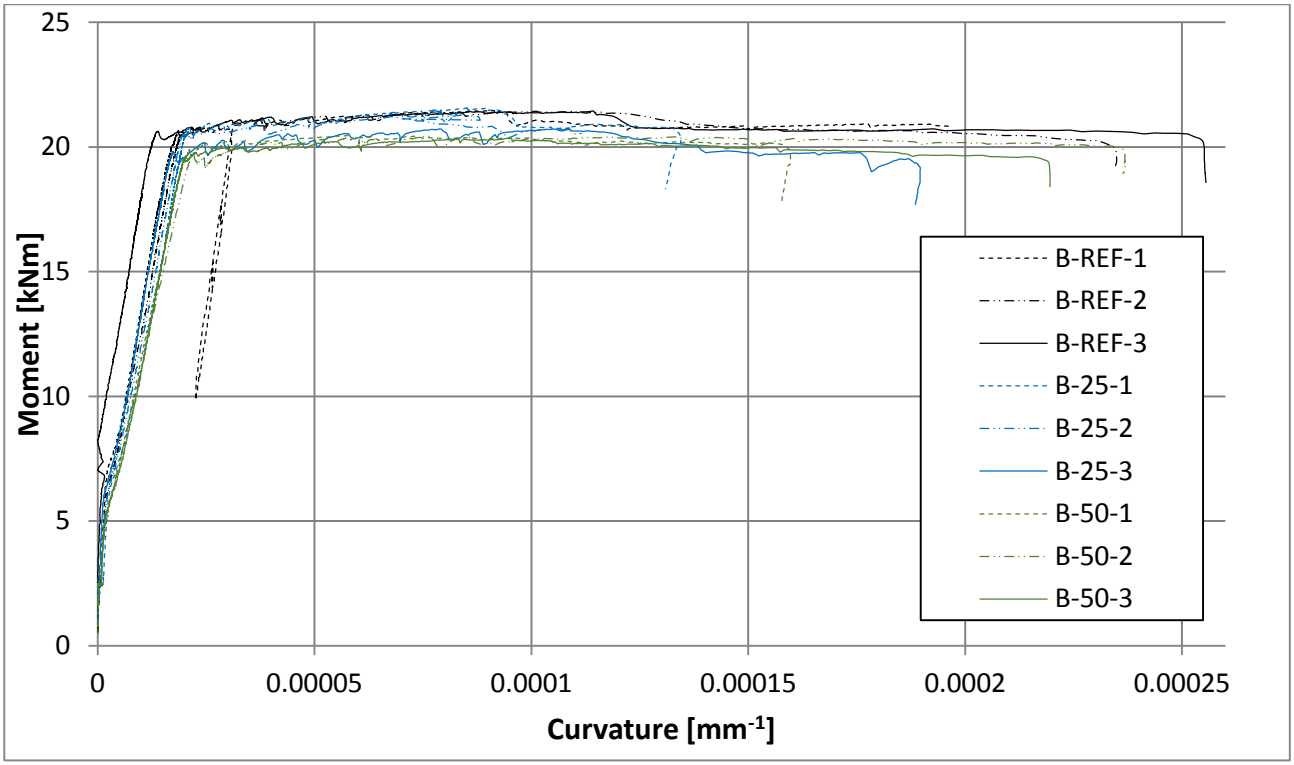

Figure 4-12: Moment-curvature curves for all tested beams.

It is observed that the beams generally have very ductile and similar behavior. They obtain large increases in curvatures when reaching the moment capacity before fractures occur in the concrete compressive zone. This type of behavior is characteristic for normal reinforced beams and it can be concluded that the ductile behavior of the beams is independent of the SSA content in the concrete. It is observed that the beams have similar moment capacities; however a small decrease is observed for increased SSA content. In the elastic part of the moment-curvature relation it is observed that the beams have similar behavior and the moment-curvature relationship varies very little. The exception is the beam B-REF-3 that indicates to have a moment of almost 10kNm before any curvature is registered. This is referred to as a fault with the displacement measurements in that experiment resulting in a dislocation of the curve, and not a different stiffness of the beam.

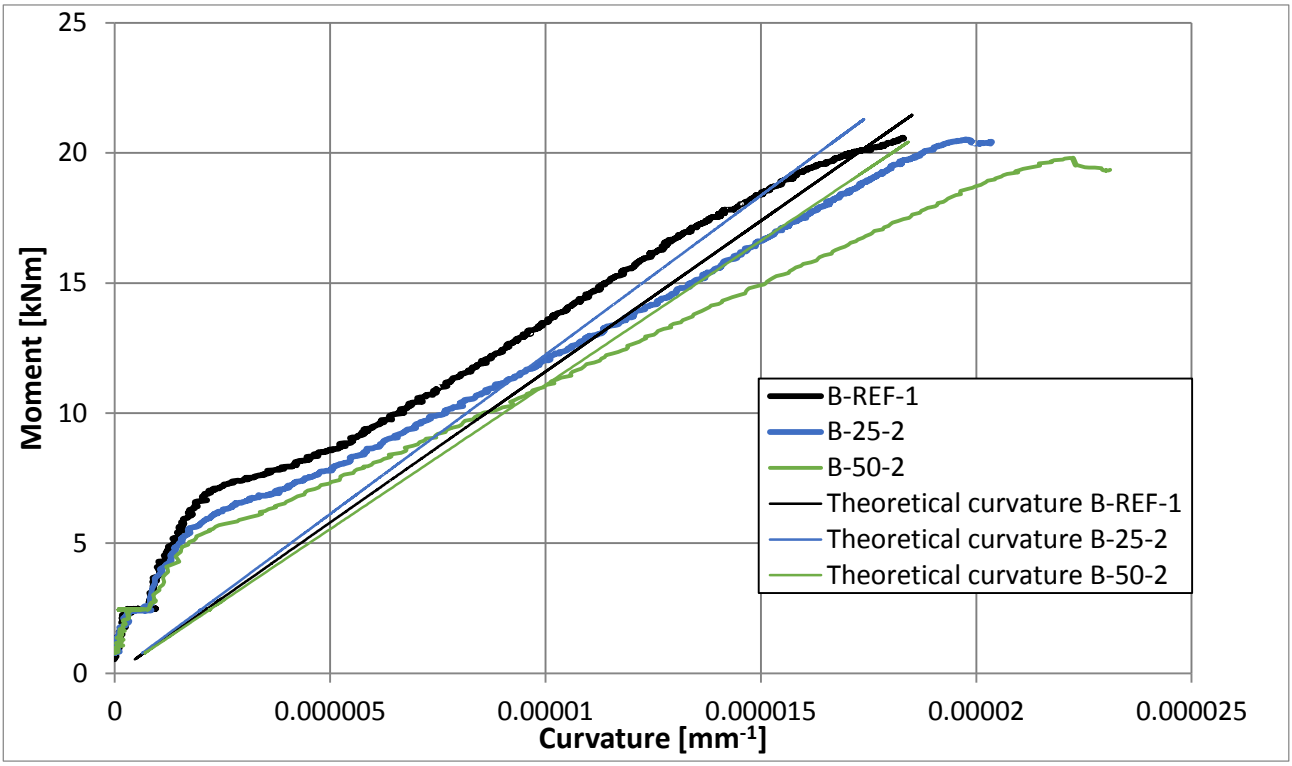

Figure 4-13: Elastic parts of moment-curvature curve for representative beams, along with theoretical

In Figure 4-13 three representative moment curvature curves have been presented along with theoretical moment curvature relationships for the respective beams in the elastic parts of the curves. For the reference beam the curvature for a given moment is overestimated for the entire elastic part of the moment-curvature curve. For the SSA beams the curvature is overestimated for the first half of the elastic part of the moment curvature curve, and underestimated for the second half of the elastic part of the moment-curvature curve for a given moment. The theoretical calculation however is based on the fully cracked cross section which explains the overestimation of the curvature in especially the beginning of the curves where the cross sections are not actually cracked. For the SSA beams the underestimation of the curvature for a given moment might lie in the Young's modulus of the concrete. It has not been investigated how the SSA influence the Young's modulus of the concrete, but it is possible that it reduced more than would be expected from the reduction of the compression strength.

4.9.3 Crack distances

The crack distances are measured between the load point where the moment is constant and compared to the theoretically calculated max crack distances.

	Mean experimental crack distance [mm]	Experimental standard deviation [mm]	Characteristic max crack distance (95% percentile) [mm]	Theoretical max crack distance [mm]
B-REF-1	101.8	11.2	120.2	191.19
B-REF-2	103.0	10.8	120.8	195.69
B-REF-3	100.1	12.0	119.8	196.92
B-25-1	99.9	27.7	145.5	190.21
B-25-2	101.5	19.6	133.7	195.10
B-25-3	99.4	12.6	120.1	194.38
B-50-1	99.4	29.2	147.4	187.78
B-50-2	93.5	16.6	120.8	191.07
B-50-3	107.8	22.9	145.5	194.80

It is observed that the mean crack distances in the experiments are significantly lower than the theoretically calculated max crack distance. When comparing the upper characteristic value for the experimentally observed cracks with theoretically calculated max crack distance the difference is large. It is however observed that all the mean crack distances are approximately the same as the distance between the stirrups between the load points. This suggests that the stirrups are an indicator for crack initialization. The cross section of the concrete is reduced at the stirrups. This reduces the tensile capacity of the concrete at these sections leading to crack initialization.

4.10 Source of errors

In some of the four point bending experiments it was observed that the extensometers at large deflections in the beam experienced rotation about their fixation point resulting in smaller measured displacement than actually happening. By measuring the maximum angle in AutoCAD from a screen shot of the extreme point a maximum rotation of 11° was observed. The error can then be calculated as

$$\cos(11°) = 0.982$$

This means that maximum error in the measured displacement is 1.8% it has been decided not to correct the post-processing of the measured displacement for this error, as it only happened on some of extensometers and only in last part of the plastic deformation of the beams. Furthermore the error is concluded to be too small to influence the results significantly.

Figure 4-14: Maximum deviation angle of extensometers for beam experiments at maximum displacements

4.11 Sub-conclusion four point bending tests

Based on the behavior of the beams presented in the moment-curvature charts it is concluded that is possible to use SSA to replace cement in reinforced concrete beams without experiencing dramatic losses of moment capacity in the beams. The failure of the beams using SSA concrete is considered ductile, and will yield large visible deflections before concrete compression failure occurs.

5 Column experiments

A column is basically a beam loaded in the axial direction. Columns can then be either centrically or eccentrically loaded. In constructions most concrete columns are considered eccentric loaded due to the geometry of buildings and imperfections. In this project eccentric loaded columns are investigated.

5.1 Calculation theory

Assumptions:
Geometric condition: Plane cross sections remain plane. Meaning strain distribution is linear in cracked as well as uncracked situation.

Physical condition: Reinforcement steel is considered ideal as shown in Figure 3-2. The compression zone is considered to have rectangular uniform stress in the height of the plastic part of the compression zone shown in Figure 5-1 and completely cracked in the tension zone.

Static condition: The section forces are in equilibrium.

The calculation takes all reinforcement into consideration.

The experimentally determined material properties for reinforcement steel and concrete are used in the calculations. Mean values are used, and no partial coefficients are used

The nominal dimensions of the columns are used in the calculations, and tolerances have to be taken into account.

The eccentricity of the normal-force is set to $e = 40mm$.

5.2 Theory of eccentric loaded column

The eccentric loaded column is based on a plastic distribution shown in Figure 5-1. The principle behind the determination of the capacity is to set up two expressions for the normal capacity of the cross-section as a function of the steel strain and solve these as two equations with two unknowns.

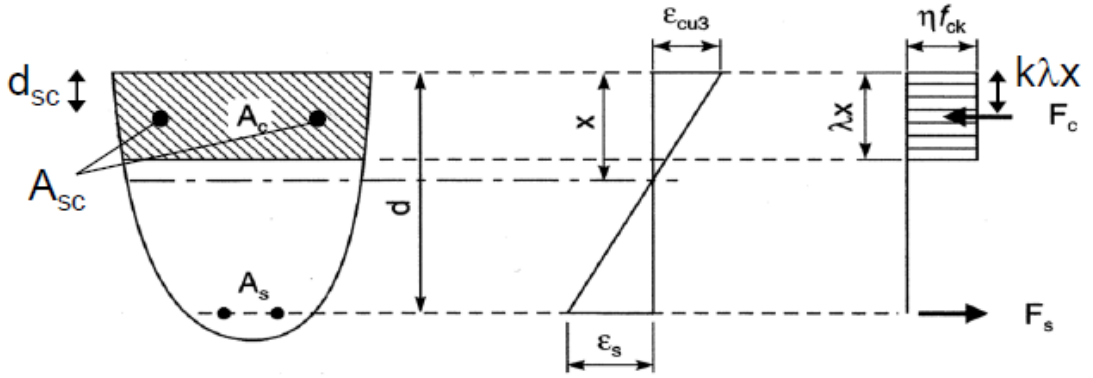

Figure 5-1: Stress/strain relation for the plastic distribution of the cross-section. [18]

The initial guess for the deflection based on a cracked cross-section is defined as a function of the buckling length L_s

$$u = \frac{1}{10}\frac{\varepsilon_{cu3} + \varepsilon_s}{d} L_s^2 \tag{5-1}$$

The strain in the compression reinforcement is then defined by looking at the strain relation in Figure 5-1.

$$\varepsilon_{sc} = \varepsilon_{cu3} - (\varepsilon_{cu3} + \varepsilon_s)\frac{d_{sc}}{d} \tag{5-2}$$

Now the stress in the compression reinforcement is determined depending on the strain

$$\begin{aligned} \varepsilon_{sc} < 0: \qquad & \sigma_{sc} = \max\begin{cases} -f_y \\ \varepsilon_{sc} E_s \end{cases} \\ \varepsilon_{sc} \geq 0: \qquad & \sigma_{sc} = \min\begin{cases} f_y \\ \varepsilon_{sc} E_s \end{cases} \end{aligned} \tag{5-3}$$

And the stress in the tension reinforcement

$$\sigma_s = \min\begin{cases} f_y \\ \varepsilon_s E_s \end{cases} \tag{5-4}$$

The height of the plastic compression zone y of the concrete can be determined through Figure 5-1, where $\eta = 0.8$ for rectangular compression zones.

$$y = 0.8x = 0.8\frac{\varepsilon_{cu3}}{\varepsilon_s + \varepsilon_{cu3}} d \tag{5-5}$$

Yielding the plastic compression area $A_{cp} = y \cdot b$.
Through equilibrium of the forces the normal capacity can then be expressed as:

$$N_1 = A_{cp} f_{cm} - A_s \sigma_s + A_{sc} \sigma_{sc} \tag{5-6}$$

Yielding the second order moment of the column

$$M_1 = N_1(e + u) \tag{5-7}$$

The second expression is then determined by considering the moment equilibrium of the forces

$$M_2 = A_s \sigma_s \left(d - \frac{h}{2}\right) + A_{sc} \sigma_{sc} \left(\frac{h}{2} - d_{sc}\right) + A_{cp} f_{cm} \left(\frac{h}{2} - \frac{y}{2}\right) \tag{5-8}$$

And thus the normal capacity

$$N_2 = \frac{M_2}{e + u} \tag{5-9}$$

The solution is then obtained by solving $M_1 = M_2$ or $N_1 = N_2$. The results for a variety of different parameters are shown in Table 5-1.

5.3 Results from theoretical calculations

In Table 5-1 the theoretical results are shown.

Table 5-1: Theoretical results

Beam No.	Moment [kNm]	Normal force [kN]	Tensile Steel strain ε_s [‰]	Deflection [mm]
S-REF-1	17.7	183	7.4	54.4
S-REF-2	17.9	192	7.3	52.8
S-REF-3	17.8	191	7.4	53.5
S-25-1	18.2	212	5.9	46.0
S-25-2	18.1	210	5.9	46.2
S-25-3	18.5	217	5.9	45.4
S-50-1	16.5	231	3.0	31.9
S-50-2	16.7	234	3.0	31.7
S-50-3	16.8	234	3.0	31.8

It is observed that the normal force increases when more SSA is added in the calculation. This is related to the deflection which decreases when more SSA is added. A smaller deflection means a smaller eccentricity, which leads to a smaller moment for the same normal force. This results in a larger axial capacity before moment failure occurs in the columns. The compressive strength of the concrete is lower when adding SSA. This will result in a somewhat constant moment in the columns.

5.4 Cracks

The distance between the cracks is calculated with (4-16) and (4-17). In Table 5-2 the distances between cracks are shown along with the deviations from the reference and the deviation from the criteria (4-18).

Table 5-2: The distance between cracks for the three series.

	Cracks		
	[mm]	Dev. from ref	Dev. from criteria
S-REF	185.4	0.00%	9.36%
S-25	184.9	-0.26%	9.67%
S-50	181.9	-1.86%	8.22%

Even though the criterion is not fulfilled the estimation of distances is still used as no other method is found. The deviations from the criteria are all under 10%, why it is assumed that the results are adequately accurate.

5.5 M-N Diagram

In a column it is necessary to design for both the normal force N and the moment M from eccentricities and deflection during longitudinal loading. Regarding load carrying capacity for a column, the relation between M and N is plotted in a graph. The experimentally determined results of M and N are then plotted in the same graph, to see where how the relation between M and N is at failure. With the method used in section 5.2 it would only obtain one point on the graph, where there in reality are many combinations of the normal force and moment. The method in section 5.2 is based on an elastic deflection of the column. It is not suitable for estimation of the ultimate capacity, where plastic deflections are present. Therefore this M-N diagram is plotted with the deflection determined experimentally. An example of a M-N diagram is shown in Figure 5-2.

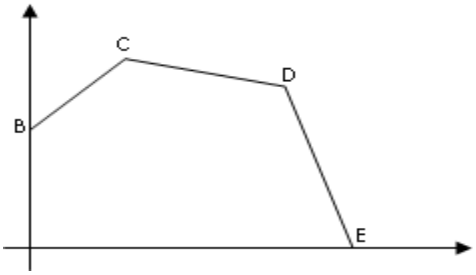

Figure 5-2: Sketch of N-M diagram.

M an N are found by the equations presented in section 4.2.1.
The equations are solved by what-if analysis in excel in the following way:

In point B the column is only subjected to bending i.e. the moment is found by varying the height of the compression zone (x) while keeping the axial force zero.

In point C the cross section is balanced meaning that there will be crushing in the outermost concrete, and yielding will just be obtained in the reinforcement. Moment and normal force is found by keeping the strain in the reinforcement constant at the yielding strain $\varepsilon_s = \varepsilon_y$ while varying x.

Point D is crushing in the concrete compression zone and zero strain in the reinforcement $\varepsilon_s = 0$.

Point E is found by solving equation (5-6) for the normal force. The moment is equal to zero.

$$N = b \cdot h \cdot f_{cm} + (A_s + A_{sc}) \cdot \sigma_s \tag{5-10}$$

Where the steel stress is:

$$\sigma_s = \min\begin{pmatrix} E_s \cdot \varepsilon_{cu.2} \\ f_y \end{pmatrix} \tag{5-11}$$

5.6 Sensitivity analysis column tests

To analyze the sensitivity of the M-N diagram calculations, experimentally determined material properties are changed to their extreme values, which is the limits of 95% confidence interval. These are obtained by (4-19).

The properties under consideration are:

- Concrete compressive strength
- Yield stress of reinforcement steel
- Young's modulus for the reinforcement steel
- Cover thickness is varied +/- 5 mm from the mean cover as it correspond to the tolerance
- $\varepsilon_{cu3}/\varepsilon_{cu2}$ – Depending if the cross-section is in bending or compression, are varied +/- 0.5‰

In Figure 5-3, Figure 5-4 and Figure 5-5 the M-N diagrams for the mean value are plotted as the solid line. The dashed lines are M-N diagrams where all five properties are changed to their upper and lower extreme values respectively. The dotted line is showing the concrete compressive strength as the only varying parameter. Lastly the experimental results are also plotted as points.

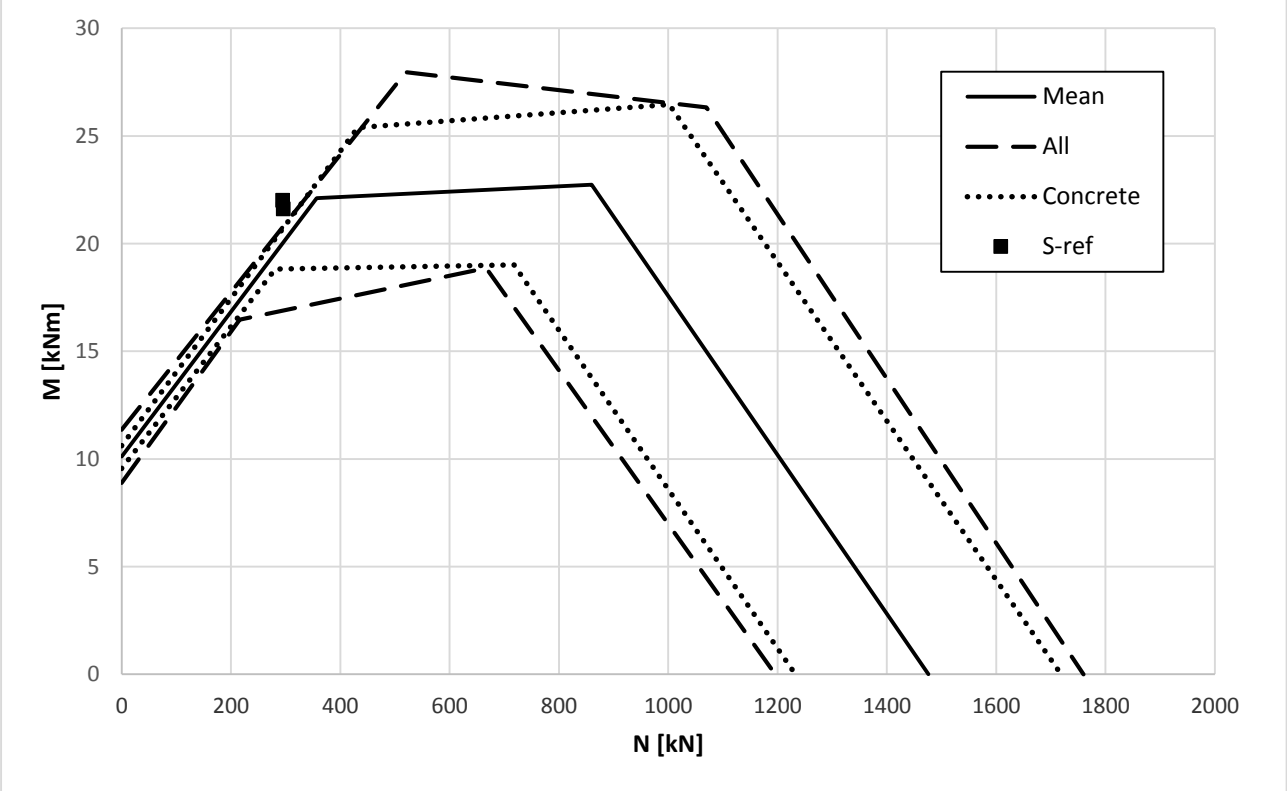

Figure 5-3: Sensitivity analysis for the S-REF series

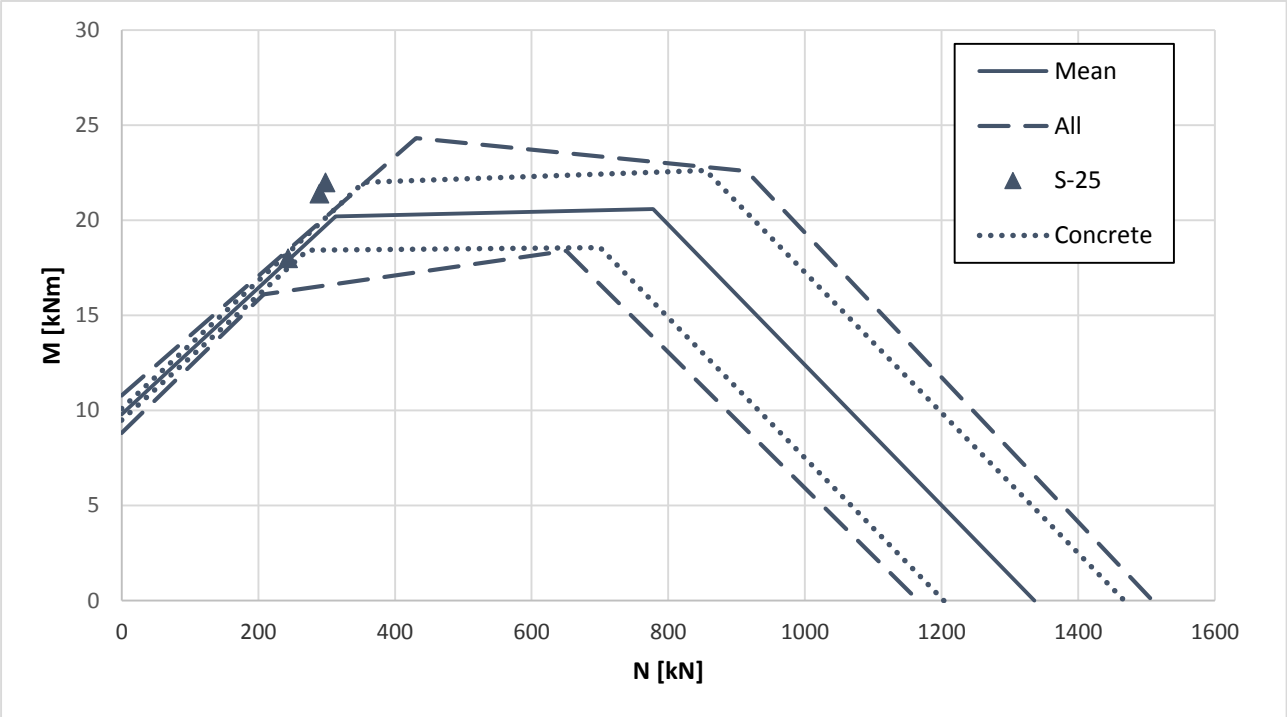

Figure 5-4: Sensitivity analysis for the S-25 series.

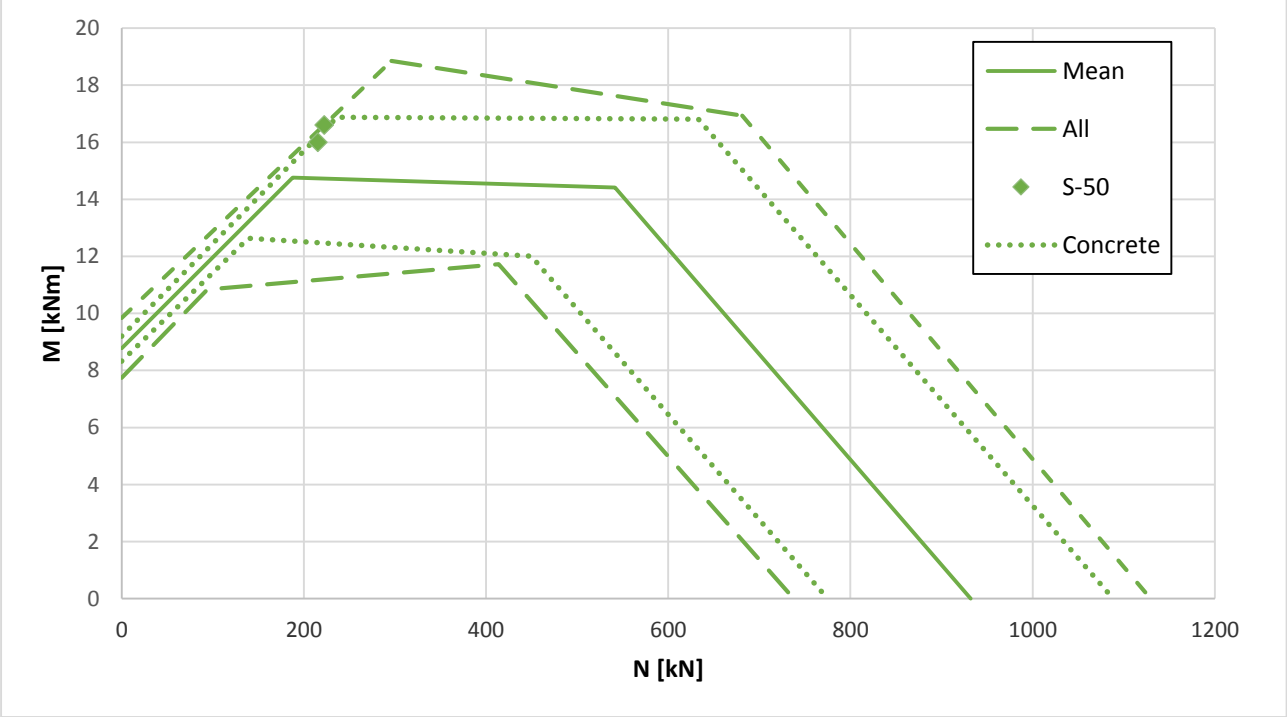

Figure 5-5: Sensitivity analysis for the S-50 series

The concrete curves are included in these charts. This is to illustrate that the dispersion when testing the concrete compressive strength is the most influential parameter when performing sensitivity analysis. The concrete compressive strength is responsible for most of the dispersion with the M-N curves, whereas the 4 other parameters checked are responsible for a small part together. This is expected since the concrete is an inhomogeneous material, which leads to a larger dispersion. The performed sensitivity analysis is deemed satisfactory as the dispersion within the concrete compression strength is a known factor. The influence of the individual parameters is shown in appendix H.

5.7 Column production

The mixing and casting of the columns are similar to mixing and casting of the beams, why it is not repeated in this section. The procedures are described in section 4.5.

5.8 Experimental setup column test

When the columns have reached the desired maturity, they are tested to find axial load capacity. The test machine is a custom made compression machine where the compression is in the horizontal direction. This test setup eases the mounting and de-mounting of the columns compared to a test setup with compression in the vertical direction. The horizontal test setup also ensures a higher degree of safety as the columns will not be able to fall out of the rig in an uncontrolled direction after failure. The test setup is shown in Figure 5-6Figure 4-5.

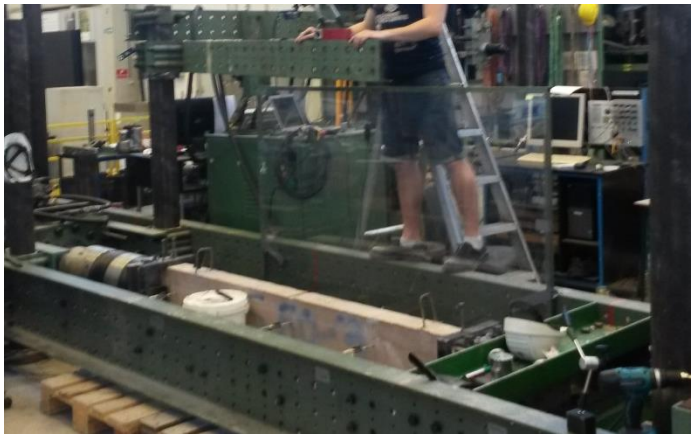

Figure 5-6: General view of column setup.

Figure 5-7: Column hinged support.

During loading the column deflects and form a curvature, thus it is necessary to have supports which are able to rotate to maintain the same stress distribution throughout the cross section. In Figure 5-7 this hinged support is shown. The column is fitted in the support with an eccentricity by which the direction of the deflection can be controlled. The eccentricities at the supports are adjusted, see Figure 5-8 and Figure 5-9.

Figure 5-8: Support (Right side) for the eccentricity.

Figure 5-9: Support (Left side) for the eccentricity.

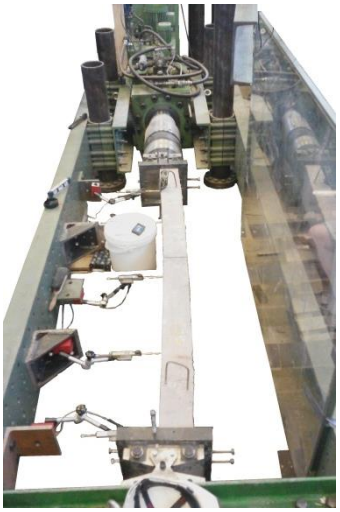

Figure 5-10: Position of the electronic extensometers.

Magnetic stands with electronic extensometers are placed at five points in the longitudinal direction of the column as shown in Figure 5-10. The extensometers are connected to a data logger along with the applied axial load and the axial displacement.

On the control panel, the load program is set up. A single step is needed and the load rate is determined to be about 5% of the initially estimated ultimate load per minute. The cameras are placed on a stand above the column.

5.8.1 Equipment and material column tests

- Custom made INSTRON column testing machine - 1000 kN, with mounted load cell.
- Control panel for the load program
- Data logger.
- 2 hinged supports with one rotational degree of freedom for the deflection.
- 5 electronic extensometers with 100mm potential displacement.
- Magnetic hydraulic stands to support extensometers.
- Overhead travelling crane for moving the columns.
- 2 Cameras.

5.8.2 Test procedure column tests

1. The column is marked at the points where displacements measurements are taken.
2. The column is lifted in to the supports, and the piston is moved forwards until it is loading the column with approximately 2 kN.
3. The bolts on the supports are tightened and the eccentricity of the column is adjusted to obtain $e = 40mm$.
4. The extensometers are placed on the marks; leveled and perpendicular to the column.
5. Simultaneously the logger, load program, and cameras are started.
6. The test is then performed until failure.
7. When the test is complete, the extensometers are detached, the bolts in the supports are loosened and the piston is retracted.
8. The column is lifted and removed from the test setup.
9. The crack pattern is marked and the distance between the cracks is measured.
10. With a hammer and a chisel the covering layer is removed and the distance to the longitudinal reinforcement on both the compression and the tension side are measured.

5.9 Post-processing column

5.9.1 Load

From the data logger a voltage output is obtained. To convert this to a load [kN] a factor of 120 must be multiplied.

$$F = U \cdot 120 \tag{5-12}$$

5.9.2 Displacement

The displacement is registered in electronic extensometers were a needle is able to be displaced up to 100mm, which is registered in the extensometers as a change in voltage. The voltage varies from 0 to 5 volts over the 100 mm displacement of the needle

$$\Delta s = \Delta U \cdot \left(\frac{100mm}{5V}\right) \tag{5-13}$$

5.9.3 Moment

The moment induced in the column originates from the eccentricity in the test setup, and the ongoing deflection increases with the load.

$$M = F \cdot (\Delta s + e) \tag{5-14}$$

5.9.4 Curvature

The curvature is calculated in the same way as the curvature for the beam, see section 0. In the columns a constant curvature or moment does not exist, why it is necessary to approximate a mean value for both. The curvature and moment are assumed to vary between the two intermediate extensometers and the middle extensometer in a parabola shape, shown in Figure 5-11.

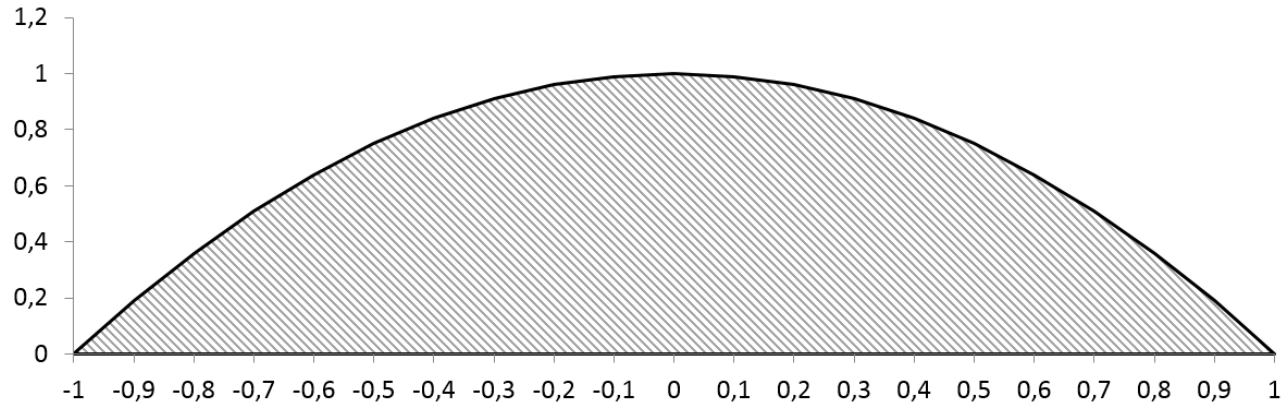

Figure 5-11: Parabola shape for the displacement, with the function: $y = -x^2 + 1$.

To obtain a mean value the area under the parabola must be determined by integration from -1 to 1:

$$\int_{-1}^{1} (-x^2 + 1)dx = \frac{4}{3}$$

To obtain a mean value the area is divided by the base length (2), leading to the mean value of 2/3^{rds}. This means that the mean value of the moment will be 2/3^{rds} of the difference between the middle extensometer and the average of the intermediate extensometers.

5.10 Experimental results columns

In this subsection the results column experiment are presented. The detailed results of each individual column is presented in appendix I.

In three of the tests, one of the extensometers did not provide the displacement data from the beginning. This is the case for the middle extensometer in S-REF-3 and S-50-2 and the intermediate extensometer in S-50-3. The reason why this happened is unclear at this point. The consequence of this error is that data regarding displacement in the respective extensometers are discarded in the three tests. Because of this, transversal displacement at midpoint and moment cannot be obtained for S-REF-3 and S-50-2. Regarding S-50-3 the erroneous data has been compensated for by replacing the logged data from the erroneous extensometer with data from the functioning extensometer. See appendix I for visualization of the errors.

Table 5-3: Key results from the column experiment.

	Axial capacity N_R		**Moment capacity M_R**		**Transverse displacement u at maximum load**		**Axial capacity compared to S-REF mean**
	Test value	Mean	Test value	Mean	Test value	Mean	
	$[kN]$	$[kN]$	$[kNm]$	$[kNm]$	$[mm]$	$[mm]$	[%]
S-REF-1	295		21.6		32		
S-REF-2	294	295	22.0	21.8	33	33	100%
S-REF-3	295		-		-		
S-25-1	289		21.4		33		
S-25-2	243	277	18.0	20.5	33	33	94%
S-25-3	298		22.0		33		
S-50-1	215		16.0		32		
S-50-2	228	222	-	16.6	-	33	75%
S-50-3	222		16.6		34		

In Table 5-3 and Table 5-4 the key results from the column experiment are presented. As expected the load capacity decreases with increasing SSA content. The decrease is not linear. The axial capacities are reduced by 6 % and 25 % for S-25 and S-50 respectively. The same tendency applies for the moment. Regarding the transverse displacement it is observed that the same displacements are obtained for all the columns. From Table 5-4 it is seen that the theoretical displacements are overestimated in the S-REF and S-25 series however fits with the S-50. It is also observed that the calculated axial capacity is underestimated for the S-REF and S-25 series.

Table 5-4: Comparison between experimental and theoretical results.

	Mean Axial capacity compared to theoretical axial capacity $\frac{N_{expe,mean}}{N_{theoretical}}$	**Maximum transverse Displacement compared to theoretical displacement** $\frac{u_{exper,mean}}{u_{theoretical}}$
S-REF	156 %	62 %
S-25	130 %	72 %
S-50	95 %	104%

The reduction in axial force capacity determined experimentally for the columns when increasing the SSA content is opposite to what the theoretical calculation shows. The answer lies in the calculation of the

deflection of the column. This deflection is used to obtain the moment with relation to the normal force, and the calculation is calculated using linear assumptions. This calculation method is used since no other solution is found. The unsuitable deflection determination is also observed when regarding the displacement both theoretically and experimentally. Theoretically the displacement decreases with a higher amount of SSA, whereas the deflection in the experiments is similar for the three types of columns. The theoretically calculated deflections are also larger or equal to the experimentally determined deflections.

For each of the nine tests a load-displacement curve at mid-span is produced. The curves are shown until failure in Figure 5-12.

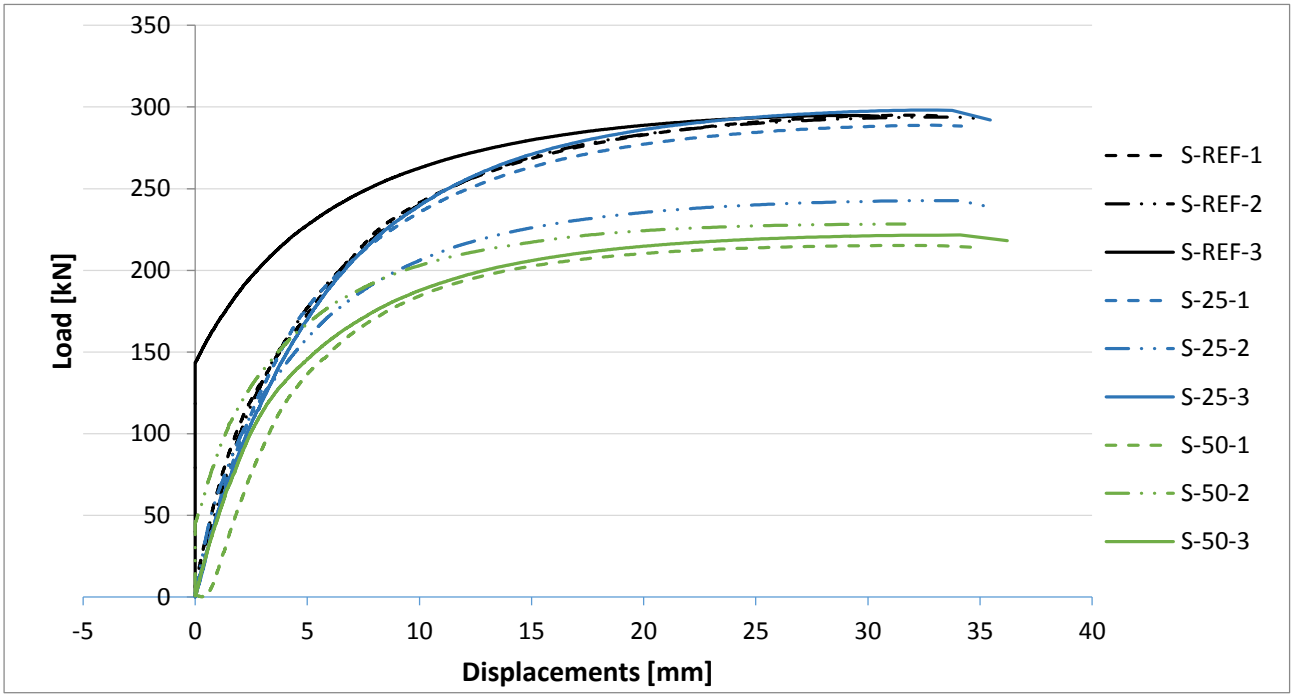

Figure 5-12: Load-displacement curve for the nine columns.

As previously mentioned the data for the two columns S-REF-3 and S-50-2 are flawed regarding displacement. These are included although the curves are displaced horizontally. The progress of the curves is as expected. Initially there is an elastic zone, which is almost linear. Afterwards a transition zone leads to a plastic zone. Regarding the S-25 series, the deviation is significant. S-25-1 and S-25-3 are close to the load capacity of the reference series whereas the S-25-2 column is closer to the S-50 series.

In Figure 5-13 the erroneous data is recognized. For the S-50-3 a revised version is made cf. the top of this section.

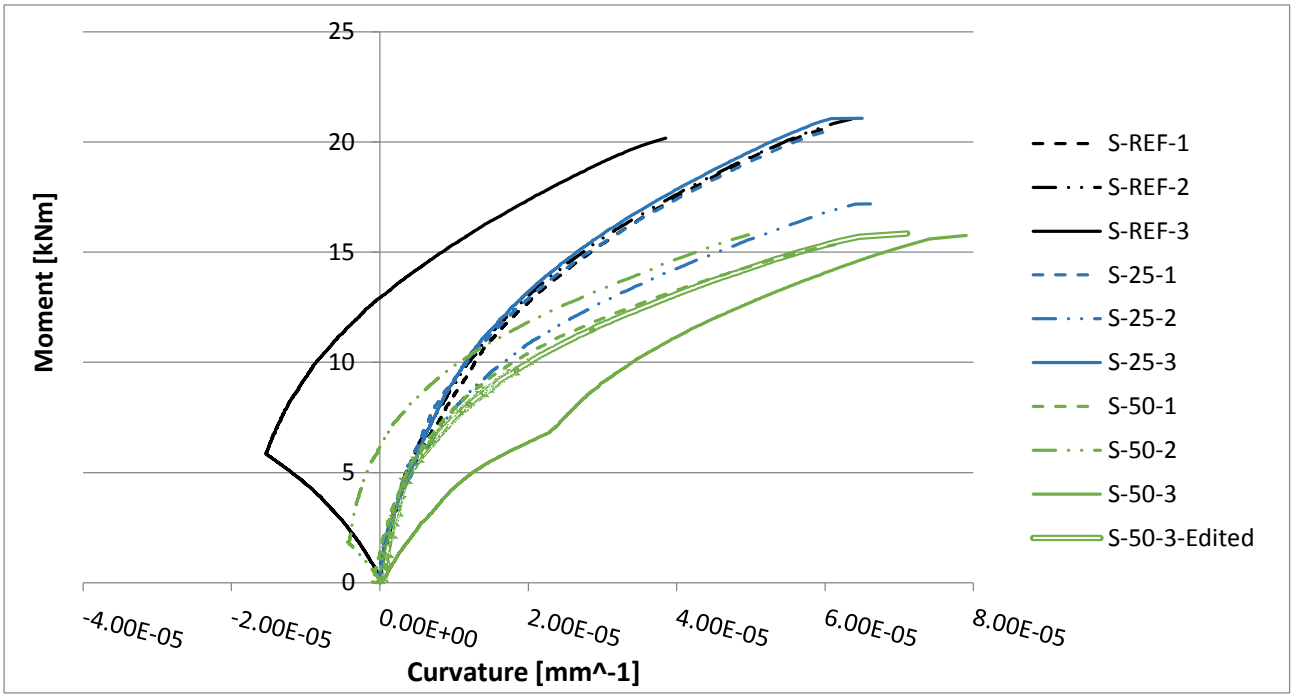

Figure 5-13: Moment-Curvature curves for the nine columns.

The tendency, that applies for the Load-Displacement chart, also applies for the Moment-Curvature chart. The S-REF shows the largest moments, which means this series will have a higher moment at the same curvature in relation to the other series. The S-50-series shows the smallest moments on the graph, and the S-25-series is in between, as on the Load-Displacement curve. In Figure 5-12, Figure 5-13and Figure 5-14 it is observed that S-25-2 is lower than the other columns in this series. This column has been measured and mixed together with the rest of the series, and kept under the same conditions. The deviations could be related to differences during the casting process including vibration. Also a local weakness in the concrete could be responsible, or more likely a combination of these events. It was observed that plastic pieces from the concrete mixer broke off during the mixing and ended up in the concrete. However no definitive answer is found for this problem.

The columns show sufficient ductility to be categorized as normal reinforced. Generally the columns show more ductility when the SSA content is increased, as they obtain larger curvatures at failure.

5.10.1 M-N Diagram

To see how the relation between moment and normal force is, the failure loads are plotted in a M-N diagram, Figure 5-14.

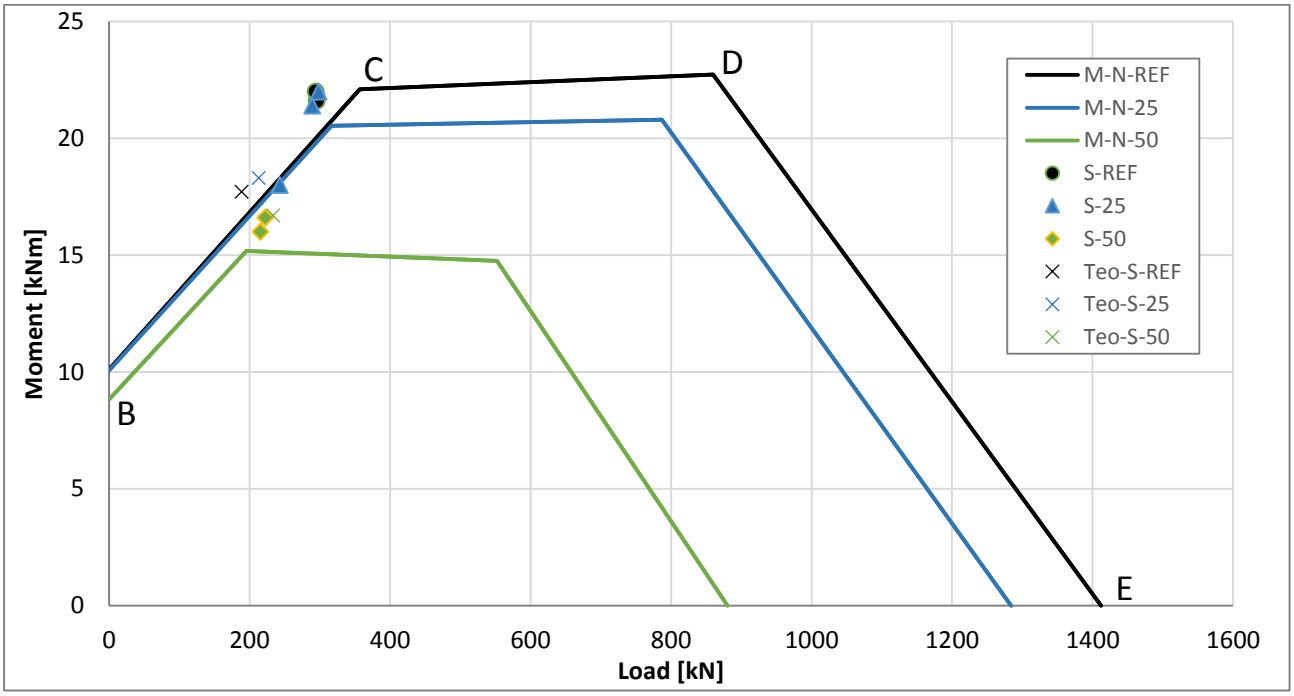

Figure 5-14: M-N diagram for the columns, REF-3 and 50-2 are excluded due to flawed data.

In Figure 5-14 it is observed that the S-50 series is situated close to point C on the M-N-50 curve. The same applies for two of the points in the S-25 series. The last point in the S-25-series deviates from the other two, which is also observed in Figure 5-12 and Figure 5-13. For the S-REF series it is observed that the points are not near the point C on the curve, however they are near the line BC of the curve.

In the M-N diagram Figure 5-14, it is observed that all the test results (except S-25-2) are located outside the M-N-curve. This could indicate that the calculation method used for this project is conservative. The results are near the moment axis, to the left of point C. This position in M-N diagram is desirable as centrically loaded columns (positioned near point E) have a tendency to fail by local crushing at the ends.

5.10.2 Crack distance

Table 5-5: Mean crack distances measured in the tests

	Mean experimental crack distance [mm]	Experimental standard deviation [mm]	Characteristic max crack distance (95% percentile) [mm]	Theoretical max crack distance [mm]
S-REF-1	98.4	19	129.6	185.4
S-REF-2	97.2	24	136.7	185.4
S-REF-3	79.6	20.3	113.0	185.4
S-25-1	99.9	17.6	128.9	184.9
S-25-2	101.5	20.8	135.8	184.9
S-25-3	99.9	17.6	128.9	184.9
S-50-1	91.4	20.5	125	181.9
S-50-2	99.4	10.9	117.4	181.9
S-50-3	98.1	15.3	123.2	181.9

It is observed that the mean crack distances in the experiments are significantly lower than the theoretically calculated max crack distance. When comparing the upper characteristic value for the experimentally observed cracks with the theoretically calculated max crack distances the differences are large. It is observed that all the mean crack distances are approximately the same as the distance between the stirrups between the load points. This suggests that the stirrups are an indicator for crack initialization in the same manner as for the beams. The cross section of the concrete is reduced at the stirrups. This reduces the tensile capacity of the concrete at these sections leading to crack initialization.

5.11 Sub-conclusion column tests

It is concluded in the column experiments that the axial capacity of the S-25 series decreases with 6 % and the S-50 series with 25 %. The displacement at mid span for maximum axial capacity is similar regardless of how much SSA is added. The distance between the cracks is also similar regardless of SSA added, but it is concluded to be the stirrup distance that indicates crack initialization.

6 Conclusion

The scope of the project is to determine if sewage sludge ash is viable as an additive replacing part of the cement in concrete structures.

It is concluded that replacing part of the cement up to 50% of the weight with SSA, reduces the compressive strength of the concrete. With this reduction in compressive strength the concrete still fulfills the requirement for constructions in passive exposure class. It is therefore a viable choice when designing structures in this exposure class. It is also concluded that using lower SSA content (25 %) leads to minor reductions of concrete compressive strength. This indicates that even in constructions where a high compressive strength is required, SSA can replace part of the cement in the concrete.

It is concluded based that beams made with a SSA replacement of cement of up to 50% by weight does not experience significant reduction in moment bearing capacity. It can therefore be concluded that SSA concrete is very useful in beam structures, primarily exposed to bending.

It is concluded that the calculation methods for the bearing capacity of beams are accurate for normal reinforced beams.

It is likewise concluded that columns made with a SSA replacement of cement of up to 50% by weight is possible to use. The reduction in concrete compressive strength does however influence the axial capacity of eccentrically loaded columns, why it is necessary to design columns with this fact in mind.

It is concluded that the calculation method for the deflection of columns to determine the moment in an eccentrically loaded column is inaccurate. The deflection at failure yields plastic deformations in the reinforcement which is not accounted for in the equation. A better method to assess the limits of the bearing capacity of columns is M-N diagrams.

It is observed that the workability of the concrete is reduced when replacing cement with SSA. This indicates that the SSA increases the water demand of the concrete. This problem can partly be solved by adding super plasticizers, but a significantly lower slump should still be expected for SSA concretes compared to regular concretes.

It is concluded that the SSA content does not influence the crack distance. Indications imply that the stirrups initialize cracking.

It is concluded that the use of SSA can potentially reduce the CO_2 footprint of the concrete produced with SSA by 50%. It is concluded that the perspectives for using SSA in concrete has a huge potential in reducing CO_2 footprint as it will find use in up to 2/3^{rds} of all concrete structures produced in Denmark. This will result in total reduction in CO_2 footprint of 600.000 tons on a national scale each year

7 Future investigations

This project will be the first in a line to determine the behaviour of SSA in concrete, thus more investigations are needed before the product is ready to go on the market. Some investigations are suggested below

- Expanded investigation, to obtain a bigger statistical significance
- An investigation concerning the rheology, especially regarding the water demand of the SSA
- Expansion of Bolomey's model to design a concrete – i.e. a determination of an equivalent W/C-ratio.
- Determination of a model, which can assess the plastic deflection of a column, resulting in a correct ultimate carrying capacity of the column.
- Investigation of other ashes, from other waste water treatment plants and wooden ash.
- The durability of concrete when ash is added.

8 Bibliography

[1] International Energy Agency, World Buisness for Sustainable Development, "Cement Technology Roadmap," 2009.

[2] Betonindustriens Fællesråd, Aalborg Portland A/S, Teknologisk institut, Miljøvenlig betonproduktion, Miljøstyrrelsen, 2006.

[3] N. Mahasenan, S. Smith and K. Humphereys, "The cement and global climate change: Current and potential futute cement industry CO2 emissions," *Greenhouse Gas Control Technologies*, vol. 1 & 2, pp. 995-1000, 2003.

[4] Energistyrelsen, DS/EN 1992-1-1 DK NA:2013, Standard distribute, 2013.

[5] T. Henriksen, L. Juel-Hansen and D. Mathiesen, Udredning af teknologiske muligheder for at genbruge og genanvende beton, Miljøstyrrelsen, 2015.

[6] WBCSD & IEA, "Cement Technoilogy Roadmap 2009 - Carbonemissins reductions up to 2050," World Buisness Council for Sustainable Devolpment & International Engergy Angency, Paris, 2010.

[7] United Nations, Department of Economic and Social Affairs, "World Population Prospects: The 2012 revision," New York, 2013.

[8] L. M. Ottosen, P. E. Jensen and G. Kirkelund, "Extracting phosphorous from incinerated sewage sludge ash rich iron and aluminum.," *Chemosphere*, pp. 91:963-969, 2013.

[9] A. D. Heerholdt, P. Nepper-Christensen, C. F. P. Justesen and A. Nielsen, Beton-Bogen 2. edition, Aalborg: Aalborg Portland, 1985.

[10] H. K. Kurt, E. Linnet, A. Nielsen , M. Geiker and P. Hoffmeyer, Bygningsingeniørens materialer - uddrag af Materialebogen 1.edition, Kongens Lyngby: Nyt Teknisk Forlag, 2008.

[11] Danish Standards, "DS-EN 12350-2 Testing fresh concrete - Part 2: Slump-test," Standard distribute, 2012.

[12] "DS/EN 12390-3 + AC - Testning of hardened concrete - Part 3: Compressive strength of test specimens.," Standard distribute, 2012.

[13] Danish standard, "DS-EN ISO 6892-1-2013 Metallic materials - tensile testing - Part 1: Method of test at room temperature.," Standard distribute, 2013.

[14] P. Goltermann, "betonkonstruktioner - Department of civil engineering - Tecnical University of Denmark," 12 03 2015. [Online]. Available: http://www.betonkonstruktioner.byg.dtu.dk.

[15] Danish standards, DS-En 1992-1-1 Eurocode 2: Design of concrete structures - Part 1-1: General rules and rules for buildings., Standard distribution, 2008.

[16] M. R. Iskau and P. S. Jensen, "Design of overreinforced concrete beams," DTU byg, 2014.

[17] B. C. Jensen, Teknisk Ståbi, Nyt Teknisk Forlag, 2011.

[18] B. C. Jensen, Betonkonstruktioner efter DS/EN1992-1-1, Nyt Teknisk Forlag, 2008.